

Galaxy formation in the *Planck* cosmology – IV. Mass and environmental quenching, conformity and clustering

Bruno M. B. Henriques,^{1,2★} Simon D. M. White,² Peter A. Thomas,³
Raul E. Angulo,⁴ Qi Guo,⁵ Gerard Lemson^{2,6} and Wenting Wang⁷

¹*Institute for Astronomy, ETH Zurich, CH-8093 Zurich, Switzerland*

²*Max-Planck-Institut für Astrophysik, Karl-Schwarzschild-Str. 1, D-85741 Garching b. München, Germany*

³*Astronomy Centre, University of Sussex, Falmer, Brighton BN1 9QH, UK*

⁴*Centro de Estudios de Física del Cosmos de Aragón, Plaza San Juan 1, Planta-2, 44001, Teruel, Spain*

⁵*Partner Group of the Max-Planck-Institut für Astrophysik, National Astronomical Observatories, Chinese Academy of Sciences, Beijing 100012, China*

⁶*Department of Physics and Astronomy, The Johns Hopkins University, Baltimore, MD 21218, USA*

⁷*Department of Physics, Institute for Computational Cosmology, University of Durham, South Road, Durham DH1 3LE, UK*

Accepted 2017 April 25. Received 2017 April 25; in original form 2016 November 7

ABSTRACT

We study the quenching of star formation as a function of redshift, environment and stellar mass in the galaxy formation simulations of Henriques et al. (2015), which implement an updated version of the Munich semi-analytic model (L-GALAXIES) on the two Millennium Simulations after scaling to a *Planck* cosmology. In this model, massive galaxies are quenched by active galactic nucleus (AGN) feedback depending on both black hole and hot gas mass, and hence indirectly on stellar mass. In addition, satellite galaxies of any mass can be quenched by ram-pressure or tidal stripping of gas and through the suppression of gaseous infall. This combination of processes produces quenching efficiencies which depend on stellar mass, host halo mass, environment density, distance to group centre and group central galaxy properties in ways which agree qualitatively with observation. Some discrepancies remain in dense regions and close to group centres, where quenching still seems too efficient. In addition, although the mean stellar age of massive galaxies agrees with observation, the assumed AGN feedback model allows too much ongoing star formation at late times. The fact that both AGN feedback and environmental effects are stronger in higher density environments leads to a correlation between the quenching of central and satellite galaxies which roughly reproduces observed conformity trends inside haloes.

Key words: galaxies: formation – methods: analytical – methods: numerical – methods: statistical – galaxies: evolution – galaxies: high-redshift.

1 INTRODUCTION

Ever since galaxy morphologies were first systematically classified, it has been clear that the present population can be split into bulge-dominated (elliptical) and disc-dominated (spiral) systems (e.g. Hubble 1936). The first representative surveys showed that, at least in the local Universe, the split in morphology roughly corresponds to a split into active systems, where star formation occurs at a significant rate, and passive systems, where it is essentially absent. The two classes contribute comparably to the total cosmic mass density in stars, but tend to inhabit different environments,

with passive galaxies being found preferentially in dense regions (Davis & Geller 1976; Dressler 1980).

The very large and well-characterized samples provided by the Sloan Digital Sky Survey made clear that there is a characteristic stellar mass $\sim 10^{10.5} M_{\odot}$ above which galaxies are predominantly passive and below which they are predominantly star-forming (Kauffmann et al. 2003a). This mass also seems to separate galaxies in which central supermassive black holes and the associated nuclear activity play a major role from galaxies in which they are not normally present (Kauffmann et al. 2003b).

The passive nature and old stellar populations of massive galaxies led most early modellers to assume that all but the smallest galaxies assembled at high redshift (e.g. Peebles 1988). The discovery that the cosmic star formation rate density rises rapidly with redshift to a peak at $z \sim 2$ (Lilly et al. 1996; Madau et al. 1996) thus came as

* E-mail: brunohe@phys.ethz.ch

a surprise, supporting the earlier and initially unpopular suggestion that galaxy formation should be viewed as a process rather than as an event, with cosmic star formation rates peaking over a broad and relatively late redshift range (White 1989). Large observational surveys have now firmly established this behaviour, showing the median formation redshift of present-day stars to be $z \sim 1.3$ (e.g. Hopkins & Beacom 2006; Wilkins, Trentham & Hopkins 2008; Karim et al. 2011; Förster Schreiber et al. 2014). At each epoch the typical star-formation rate of active galaxies is approximately proportional to stellar mass, but the ratio of the two, the ‘specific star formation rate’ (SSFR) increases strongly with redshift (Daddi et al. 2007; Elbaz et al. 2007; Noeske et al. 2007; Karim et al. 2011). Such surveys also allow the observed population to be split into active and passive systems at each redshift, showing the fraction of passive systems to be much lower at early times than it is today (Bundy, Ellis & Conselice 2005; Faber et al. 2007; Ilbert et al. 2010; Pozzetti et al. 2010; Ilbert et al. 2013; Muzzin et al. 2013).

In hierarchical, dark matter-dominated models of structure formation, the accretion of baryons on to haloes is expected to follow that of the dark matter, and in this case strong feedback appears necessary to explain why only a small fraction of all cosmic baryons have been converted into stars. This issue was identified long ago using semi-analytic models (White & Rees 1978; White & Frenk 1991) and is closely related to the issue of why the most massive galaxies are currently almost all passive (Benson et al. 2003). Until recently, feedback effects in numerical simulations of galaxy formation were generally too weak to reduce star formation efficiencies to the observationally required levels (e.g. Guo et al. 2010). Although recent simulations do approximately reproduce star formation rates in active galaxies, they still struggle to produce sufficiently passive galaxies at high mass (Vogelsberger et al. 2014; Schaye et al. 2015). Thus, while the regulation of star formation by feedback now appears to be adequately represented, its ‘quenching’ at high mass is not.

Two distinct types of process have been proposed to quench star formation. One, purely internal to the galaxy and active primarily at high mass, is usually identified as feedback from an active galactic nucleus (AGN) although the evidence for this is largely circumstantial (Benson et al. 2003; Bower et al. 2006; Croton et al. 2006; Menci et al. 2006; Somerville et al. 2008; Schaye et al. 2010; Vogelsberger et al. 2014; Schaye et al. 2015). The other reflects interactions with the larger-scale environment, typically satellite interactions with the tidal field and intracluster medium of the host halo, as well as collisions with other satellites (Gunn & Tinsley 1976; Larson, Tinsley & Caldwell 1980; Moore et al. 1996). The implementation of such processes in semi-analytic galaxy formation models has generally combined with the assumed truncation of gas accretion to produce excessive quenching of low mass satellites (Weinmann et al. 2006; Henriques, Bertone & Thomas 2008; Guo et al. 2011; Weinmann et al. 2012). Better agreement with observation is found in recent hydrodynamic simulations (Bahé & McCarthy 2015; Sales et al. 2015). In the context of the semi-analytic models, AGN feedback acts earlier and more strongly on higher mass galaxies, with the result that their stellar populations are older at late times. Low mass galaxies are only quenched if they become satellites and, since the satellite fraction never exceeds ~ 50 per cent, many such galaxies remain star-forming until the present day.

A more detailed separation of the two kinds of effect has become possible as observed samples have become large enough to estimate the efficiency of quenching as a function of galaxy properties such as halo, stellar and bulge mass, AGN activity and various measures of environment (Kauffmann et al. 2004; Baldry et al. 2006; Wang et al.

2008; Peng et al. 2010; Wetzel, Tinker & Conroy 2012; Bluck et al. 2014; Knobel et al. 2015; Woo et al. 2015). The observational trends are often summarized in terms of increased probabilities of being quenched at higher stellar mass and at higher environmental density, with the two effects acting approximately independently. In a recent paper, Terrazas et al. (2016a) showed that current observational data indicate that galaxies of given stellar mass host systematically more massive black holes if they are quenched than if they are actively forming stars. Of the simulations they analysed, including the Henriques et al. 2015 model used in this work, only those having AGN-feedback-dependent quenching reproduced this observational trend, suggesting the possible importance of this process. It should however be noted that if the normalization of the black hole mass–stellar mass relation decreases towards late times, this might simply reflect the early quenching of massive galaxies (Caplar, Lilly & Trakhtenbrot 2015).

In Henriques et al. (2015), hereafter *Paper I*, we updated the *L-GALAXIES* model of galaxy formation to improve its representation of the observed evolution of galaxy abundance and quenched fraction as a function of stellar mass over the redshift range $0 < z \leq 3$. We also scaled the two Millennium Simulations on which the model is implemented to the cosmological parameters of Planck Collaboration (2014). In this paper we test how well this model accounts for quenching as a function of environment. In particular, we study the quenching–stellar mass relation separately for central and satellite galaxies, as well as its dependence on host halo mass and halocentric distance. We also study galaxy autocorrelations as a function of stellar mass for both star-forming and passive galaxies. In all cases we take care that the definitions of galaxy samples and of environmental measures are as close as possible to those used in the observational studies with which we compare. Finally, we test how well our model reproduces observed conformity effects, the tendency for the SSFR of satellites to correlate with that of the central galaxy they orbit.

Our paper is organized as follows. Section 2 summarizes the most relevant of the modifications introduced in the galaxy formation model by Henriques et al. (2015) showing how they affect the abundances of satellite and central galaxies as a function of star-formation activity and redshift. Section 3 focuses on how well the AGN feedback model reproduces the observed quenching of high mass galaxies as a function of stellar and halo masses. Section 4 compares recent observational data with predictions for quenched fractions as a function of environment as traced by host halo mass, by distance to the fifth nearest neighbour and by distance to the halo centre, while Section 5 studies autocorrelation functions for passive and star-forming galaxies as a function of their stellar mass. Section 6 looks at how the combined effects of AGN feedback and environment give rise to conformity between central and satellite galaxies. Finally, we draw our conclusions in Section 7.

2 THE MUNICH MODEL OF GALAXY FORMATION – *L-GALAXIES*

The *L-GALAXIES* model of galaxy formation includes prescriptions for a wide variety of physical processes in an attempt to simulate all the phenomena that shape the galaxy population. A full description of the current prescriptions, and in particular of changes made for this series of papers with respect to earlier work, was presented in the supplementary material to *Paper I*. These changes primarily affect low mass galaxies, $8.0 \leq \log_{10}(M_* [M_{\odot}]) \leq 9.5$, enhancing

their star formation at later times by (i) providing additional fuel through delayed reincorporation of gas previously ejected by supernovae (SN) (this mainly affects central galaxies); (ii) defining a threshold halo mass for ram-pressure stripping to be effective; and (iii) lowering the threshold for star formation (these two changes mainly affect satellite galaxies). The first modification, related to the reincorporation of gas ejected from SN feedback, is motivated by the need to decouple the accretion of baryons into galaxies from that on to haloes and ensure that enough gas is available to cool in low mass galaxies at late times. A similar result was found in the hydro simulations of Oppenheimer & Davé (2008) and Oppenheimer et al. (2010). The ram-pressure stripping threshold was introduced to avoid that the excessive hot gas content of intermediate mass groups in our model produces an effect on satellite galaxies that incorrectly dominates over any other environmental process. We are currently testing if an AGN feedback wind model is capable of ejecting the gas in order to eliminate the need for this threshold (Bower, McCarthy & Benson 2008; Fournier et al. in preparation).

A modification to the AGN feedback model ensures that intermediate mass galaxies ($\log_{10}(M_*[M_\odot]) \sim 10.5$) have significant star formation below $z = 2$, but are predominantly quenched by $z = 0$. Specifically, the heating rate is taken to be $\dot{E} \propto M_{\text{BH}} M_{\text{hot}}$ rather than $\dot{E} \propto M_{\text{BH}} M_{\text{hot}} H(z)$ (the form used in Croton et al. 2006 and Guo et al. 2011). Although the latter is closer to what is expected from Bondi accretion, the details of gas infall on to black holes remain uncertain and must be inferred from their impact on the properties of massive galaxies. The large parameter space of the current model has been fully explored using the MCMC method introduced in Henriques et al. (2009) and Henriques & Thomas (2010). Finally, the model is built on the Millennium simulations after scaling to the first-year *Planck* cosmology (Planck Collaboration 2014; $\sigma_8 = 0.829$, $H_0 = 67.3 \text{ km s}^{-1} \text{ Mpc}^{-1}$, $\Omega_\Lambda = 0.685$, $\Omega_m = 0.315$, $\Omega_b = 0.0487$, $f_b = 0.155$ and $n = 0.96$) and adopts the Maraston (2005) stellar populations originally introduced in the Munich model by Henriques et al. (2011, 2012). The change in stellar population model has negligible impact at the relatively low redshifts considered in this paper. Throughout the paper, the Millennium-II Simulation is used for $\log_{10}(M_*[M_\odot]) \leq 9.5$ and the Millennium Simulation for higher stellar masses. Above this mass cut, properties of galaxies are nearly identical in the two simulations. This includes the properties of their supermassive black holes which are particularly relevant for the quenching phenomena discussed in this work and for which numerical convergence is crucial (Angulo et al. 2014).

2.1 Quenching mechanisms

This paper focuses primarily on the processes that shut down star formation and result in evolution of the actively star-forming and quenched populations of galaxies. In our model, two distinct processes can cause a galaxy to move from the active to passive population: feedback from a central black hole that grows to a large mass while surrounded by a hot gas atmosphere, or becoming a satellite of a larger companion. In the following subsections, we describe the modifications introduced in Paper I that are particularly relevant to these processes. We refer the reader to the original paper for a full description of the galaxy formation modelling. It should be noted that although the fraction of passive galaxies increases steadily with cosmic time, passive galaxies can (and often do) return at least temporarily to the star-forming population if they accrete new gas (e.g. through a merger).

2.1.1 Quenching by radio mode feedback

As explained in appendix A10 of Paper I, two major processes increase the mass of black holes in our model: the quasar and radio accretion modes. The quasar mode produces no feedback, but it is responsible for the majority of black hole growth as cold gas is accreted during mergers. Radio-mode feedback results from hot gas accretion on to the black hole and is assumed to increase strongly with both black hole mass and hot gas mass. Massive galaxies typically host large black holes and are surrounded by massive hot gas haloes, so feedback is strong and eliminates further condensation of hot gas on to the galaxy. Star formation then exhausts the remaining cold gas and is quenched. Although star formation can occur subsequently if merging satellites bring in new cold gas, these massive galaxies live in massive haloes and their satellites are typically gas-poor as a result of tidal and ram-pressure stripping. As a result, most massive galaxies are quenched and their stellar masses grow primarily through merging.

The model for radio mode feedback in Paper I differs from that in Guo et al. (2011) and earlier papers by having a factor of $H(z)$ removed. This enhances feedback at later times and ensures that M_* galaxies are predominantly quenched by $z = 0$ despite forming a significant fraction of their stars at $z < 1$. The heating from feedback is taken to be proportional to the radio-mode accretion rate, which is assumed to be

$$\dot{M}_{\text{BH}} = k_{\text{AGN}} \left(\frac{M_{\text{hot}}}{10^{11} M_\odot} \right) \left(\frac{M_{\text{BH}}}{10^8 M_\odot} \right), \quad (1)$$

while the black hole mass itself is determined by quasar mode accretion in merger events according to:

$$\Delta M_{\text{BH,Q}} = \frac{f_{\text{BH}}(M_{\text{sat}}/M_{\text{cen}}) M_{\text{cold}}}{1 + (V_{\text{BH}}/V_{200c})^2}. \quad (2)$$

In these formulae, k_{AGN} , f_{BH} and V_{BH} are treated as free parameters. As a result of these assumptions, galaxies are more likely to be passive for larger values of black hole mass (M_{BH}), hot gas mass (M_{hot}), halo virial velocity (V_{200c}) and in environments where the typical mass ratio between satellites and centrals ($M_{\text{sat}}/M_{\text{cen}}$) is larger. The correlations between these and other galaxy properties, for example, bulge, stellar and halo masses, naturally induce further correlations between galaxy structure and quenching. For a complete description of such relations for Milky Way mass systems, see Terrazas et al. (2016b).

2.1.2 Environmental quenching

Low-mass galaxies are barely affected by their relatively small central black holes. On the other hand, both SN feedback and environment play a crucial role in shaping their properties. The modification of gas reincorporation introduced in Henriques et al. (2013) results in material ejected by SN feedback returning later than in previous models. As a result, star formation is significantly delayed in isolated low-mass galaxies ($8.0 \leq \log_{10}(M_*[M_\odot]) \leq 9.5$) peaking at $z < 2$ and continuing at a substantial rate down to $z = 0$. If such galaxies fall into a group or cluster, their subsequent evolution changes dramatically. They cease accreting from the intergalactic medium, the hot gas they do have is progressively removed by tidal and ram-pressure forces, and the gas ejected by supernova is permanently lost to the intracluster medium.

This combination of environmental processes has a strong impact on satellite galaxies and leads to the complete shutdown of star formation in a significant fraction of them. The overall impact was

too large in previous versions of our model (Weinmann et al. 2006; Henriques et al. 2008; Guo et al. 2011). Hot gas reservoirs were removed rapidly from satellites and star formation and then consumed the remaining gas until the assumed surface density threshold was reached. This quenched star formation in the majority of satellite galaxies, even when they retained significant amounts of cold gas. In the new model, ram-pressure is assumed to strip hot gas only in haloes above a minimum mass $\sim 10^{14} M_{\odot}$, and the gas surface density threshold for star formation is roughly halved from its earlier value. Combined, these modifications ensure that more hot gas remains in satellites and that, once cooled, more of it is converted into stars – delayed reincorporation of ejected gas provides enough fuel to low-mass central galaxies to drive star formation at late times, and our reductions in the strength of ram-pressure stripping and in the star formation threshold ensure that this is also true for a significant fraction of satellites.

It should be noted that Paper I did not change the treatment of tidal stripping of hot gas, so that large amounts of hot gas are still removed from satellites even in low-mass groups. The fact that satellites do not accrete from the Intergalactic Medium (IGM) and that their stars and cold gas can be totally disrupted by tidal forces also strongly affects their star formation efficiency. As will become clear later in this paper, even without ram-pressure stripping, our treatment of environmental processes still appears to cause too much quenching of low mass satellites near the centres of low mass groups. This affects only a small fraction of the population, however, since most satellites are relatively far from the group centre.

The probability that a galaxy is a satellite increases with environment density. This induces a correlation between quenching and environment density. The details of such dependences are affected by the specific scalings we assume for environmental effects. In particular, we assume that ram-pressure stripping happens when

$$\rho_{\text{sat}}(R_{\text{r.p.}}) < \frac{\rho_{\text{par}}(R) V_{\text{orbit}}^2}{V_{\text{sat}}^2}, \quad (3)$$

where $\rho_{\text{sat}}(R_{\text{r.p.}})$ is the hot gas density of the satellite at radius $R_{\text{r.p.}}$ from its centre, V_{sat} is the virial velocity of the subhalo at infall, $\rho_{\text{par}}(R)$ is the hot gas density of the parent dark matter halo at the current radius R of the satellite and V_{orbit} is the orbital velocity of the satellite. Hot gas is assumed to be tidally stripped at the same rate as dark matter (which is treated fully consistently in the original simulation) while stars and cold gas are stripped when the total mass density of the satellite within its half-light radius falls below the density of the halo within the pericentre of the satellite's orbit:

$$\rho_{\text{sat}}(R_{\text{sat},1/2}) < \rho_{\text{DM,halo}}(R_{\text{peri}}). \quad (4)$$

In combination, these various forms of stripping result in more efficient quenching in denser parent dark matter haloes, closer to their centres, for larger orbital velocities and for lower satellite masses.

2.2 Separation between star-forming/blue and quenched/red galaxies

In this paper we will use varying cuts to separate star-forming/blue from quenched/red galaxies in our model. Our approach is to use the same observables when selecting in the models as used in the observational studies we compare with. We do, however, adjust the dividing line so that it lies exactly at the bottom of the valley separating the two populations in the model. This will allow us to directly compare the relative numbers of galaxies in each population in the model and in the observed samples independently

of any differences on the global colour distributions arising from systematics in the stellar population synthesis or dust modelling. Figures with the different selections are presented in the Appendix.

In the next subsection and in Section 3.1, where stellar mass functions and the corresponding parameters resulting from Schechter function fits are presented, we will use the same distinction between red and blue objects as in Paper I. This corresponds to a cut at $u - r = 1.85 - 0.075 \times \tanh((M_r + 18.07)/1.09)$, at $z = 0$, and in the UVJ colour plane at higher redshifts. The division between populations is shown in Fig. A1 and corresponds to $U - V = 1.3$ and $(U - V) = (V - J) \times a(z) + b(z)$, where $a(z) = [0.28, 0.30, 0.32, 0.38]$ and $b(z) = [1.21, 1.18, 0.99, 0.79]$, respectively, at $z = 0.4, 1.0, 2.0$ and 3.0 .

Throughout Sections 3 and 4 (except for Section 3.1 mentioned above), passive and star-forming galaxies are separated in the $U - B$ versus stellar mass plane (Fig. A2), when comparing with the Peng et al. (2010) data, and using their SSFR, when comparing with the Wetzel et al. (2012) data. In detail, red galaxies are defined to have $U - B > \log_{10}(M_* [M_{\odot}]) \times a(z) + b(z)$, where $a(z) = [0.059, 0.041, 0.052]$ and $b(z) = [0.49, 0.62, 0.53]$ (respectively at $z = 0.05, 0.40$ and 0.86), and $\log_{10}(\text{SSFR}[\text{yr}^{-1}]) < -11.0$. When comparing model results to the clustering data as a function of colour from Guo et al. (2010), in Section 5.3, we select red galaxies using $g - r > \log_{10}(M_* [h^{-2} M_{\odot}]) \times 0.054 + 0.11$ (Fig. A3, top panel). Finally when comparing to observations of one-halo conformity from Wang & White (2012), in Section 6, we use $(g - r)^{0.1} > \log_{10}(M_* [M_{\odot}]) \times 0.09 - 0.18$ (Fig. A3, bottom panel).

2.3 The impact of quenching on different galaxy types – stellar mass functions for red and blue satellite and central galaxies

The two types of quenching process affect different types of galaxies differently. This can be seen in Fig. 1, which shows the evolution of the stellar mass functions for satellites (dot-dashed lines), central galaxies (dashed lines) and the two together (solid lines). Predictions are given for passive (red) galaxies in the upper panels and for star-forming (blue) galaxies in the lower panels (the separation between red and blue galaxies is described in the previous subsection). At all the redshifts considered, star-forming galaxies are predominantly centrals (the dashed lines are almost on top of the solid lines in the bottom panels). Massive red galaxies are also mostly centrals while low-mass passive galaxies are primarily satellites (top panels). Clearly, low-mass galaxies are quenched predominantly by environmental processes, and high-mass galaxies by AGN effects. The radio mode mechanism adopted in our model assumes feedback from hot-mode accretion to depend on the product of the black hole and hot gas masses, effectively setting a constant stellar mass threshold for quenching. This causes model galaxies to quench at the observed rate, at least since $z \sim 2$, and the characteristic stellar mass M_* of star-forming objects to remain approximately constant, also as observed.

In the following sections we will compare our model in detail with observations of quenching as a function of stellar mass and of a variety of measures of environment. We note that for most measures, AGN and environmental effects do not separate cleanly. This is a consequence of the strong coupling between different aspects of galaxy formation. For example, although AGN feedback is an internal process affecting massive galaxies, the growth in mass both of galaxies and of their central black holes is a strong function of environment, leading to an enhancement of AGN quenching in high-density regions, perhaps explaining the impact of environment

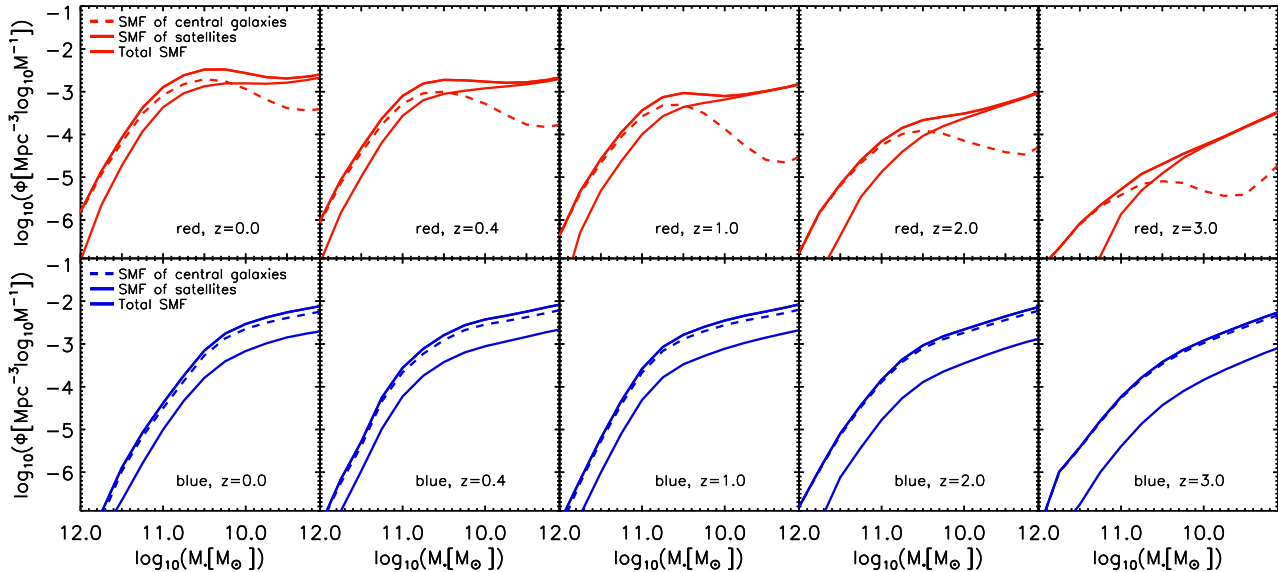


Figure 1. Evolution of the stellar mass function for all (solid lines), central (dashed lines) and satellite (dot-dashed lines) galaxies. Predictions for red and blue galaxies are shown in the top and bottom panels, respectively.

on the quenching of central galaxies recently noticed by Knobel et al. (2015). Such correlations may also be responsible, at least in part, for the observed conformity between central and satellite galaxy properties (Weinmann et al. 2006; Kauffmann, Li & Heckman 2010; Wang, Weinmann & Neistein 2012). This we will analyse in Section 6.

3 RADIO MODE QUENCHING OF MASSIVE GALAXIES

The joint dependence of the fraction of quenched galaxies on stellar mass and on environment density, as characterized by halo mass, halocentric distance, nearest neighbour distance or smoothed galaxy density, was first quantitatively established using SDSS data (Kauffmann et al. 2004; Baldry et al. 2006; Li et al. 2006; Yang, Mo & van den Bosch 2009) and was then extended to higher redshift by Peng et al. (2010, 2012). Observationally, this dependence seems to separate relatively well, with stellar mass weakly influencing quenching as a function of environment and vice versa. Separability of this kind arises naturally in semi-analytic models as a result of their representation of environmental and AGN feedback processes. Since our new model modifies the treatment of these processes in an attempt to achieve better agreement with observation, detailed and quantitative comparison with the real data is a crucial test of its success. In this section we focus on trends with stellar mass that can test our new AGN feedback implementation. In Sections 4 and 5, we focus on the impact of quenching as a function of environment and in Section 6 we will look at whether the combination of quenching effects can lead to the observed conformity between central and satellite properties.

3.1 A non-evolving stellar mass function of blue galaxies from AGN quenching

In Paper I we showed that our new model is consistent with the observed evolution of the number density of red and blue galaxies as a function of stellar mass. Fig. 2 shows the parameters resulting from Schechter function fits to the evolution of the stellar mass

function of all, of red, and of blue galaxies (the red and blue stellar mass functions are shown in Fig. 1 as solid lines). Following Peng et al. (2010), we have fit the ‘red’ and the ‘all’ mass functions with double Schechter functions assuming the same M_* for both components, whereas we fit the ‘blue’ mass function at each time with a single Schechter function (the separation between red and blue galaxies is described in Section 2.2). The same is true for the observational data at $z < 1$ while at $z \geq 1$ a single Schechter function was used for all samples. The observational data used correspond to the combined stellar mass functions used to constrain the model and were presented in figs. 2 and 7 of Paper I.

Not surprisingly, perhaps, given that the evolution of the stellar mass function and the passive fraction were the primary observational constraints on our model, the behaviour of the parameters in Fig. 2 is very similar to that which Peng et al. (2010) found in the observational data they analysed. The stellar mass function of star-forming galaxies varies little with redshift, and indeed, the three parameters combine in such a way that the actual change in the total number of objects from $z = 0$ to $z = 3$ is substantially less than the change in ϕ^* over the full range of stellar masses shown in Fig. 1. The star-forming and passive populations have similar characteristic stellar masses, M_* , which vary little with redshift, and the low-mass slopes of their dominant components, α_1 , differ by about unity and have values similar to those found by Peng et al. (2010) (in the redshift range considered in the observational study, $z \leq 1$). The normalization, ϕ^* , increases strongly with time for both components of the passive galaxy stellar mass function, and the low-mass slope of its subdominant component, α_2 , is similar to that of star-forming galaxies. Many (though not all) of these features are similar to those of the simple toy model, which Peng et al. (2010) constructed to fit their observations; the clearest differences are seen at $z \sim 2$, well beyond the redshift range $0 < z \leq 1$, where they concentrated their detailed analysis.

The rate at which massive galaxies quench can be inferred from the evolution of the massive end of the stellar mass functions. Since M_* varies little with redshift and α_1 gets shallower at late times for high-mass, passive galaxies, the evolution in their ϕ_1^* , by factors of about 300, 20 and 3 since $z = 3, 2$ and 1, respectively, is a lower

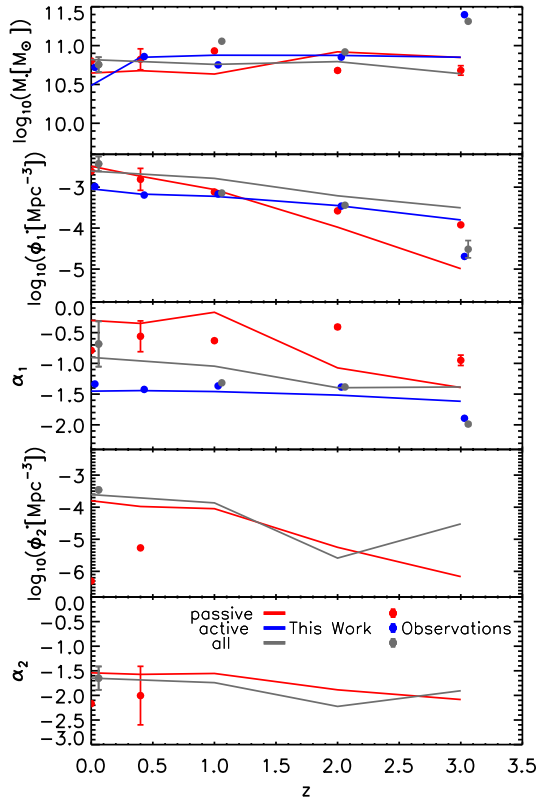


Figure 2. The evolution of the parameters of Schechter (1976) fits to the stellar mass functions of all (solid grey) passive (solid red) and star-forming galaxies (solid blue). Following Peng et al. (2010), we fit the simulation data to the sum of two Schechter functions (assumed to have the same M_*) in the first two cases, but use only a single Schechter function for the star-forming galaxies. The same is true for the observational data at $z < 1$ while at $z \geq 1$ a single Schechter function was used for all samples.

limit of the impact of the quenching process. The fact that M_* for blue galaxies is roughly constant, at least for $z \leq 1$, shows that quenching occurs with high probability once stellar masses become comparable to M_* , thereby terminating galaxy growth through star formation, and that this probability depends weakly on redshift. As Peng et al. (2010) show, it is exactly these assumptions in their toy model which enable it to reproduce the observed phenomenology. They hold approximately in our physical, Λ CDM model as a result of the way that our assumptions about AGN growth and feedback interact. Black holes grow rapidly at moderate redshift in galaxies of stellar mass $\sim 10^{10} M_\odot$ as gas-rich mergers build up their bulges. The merger products typically have haloes of mass $\sim 10^{12} M_\odot$ in which cooling times become long enough to allow the build-up of a hot gas envelope. The combination of massive black hole and hot envelope is then able to generate enough “radio-mode” feedback to cut off further cooling and quench the galaxy. For the scalings adopted in our model, the transition occurs at a halo mass and central galaxy stellar mass which are almost independent of redshift. This will be further investigated in a companion paper (Henriques et al. in preparation) and is similar to the findings of Dubois et al. (2015) and Bower et al. (2016).

It should be noted that mergers play a relatively small role in the growth of massive galaxies in this model, and hence in shaping the high-mass cut-off in the stellar mass functions. These extreme objects are mostly central galaxies in groups and clusters, where mergers contribute significant material to the intracluster stars. Nev-

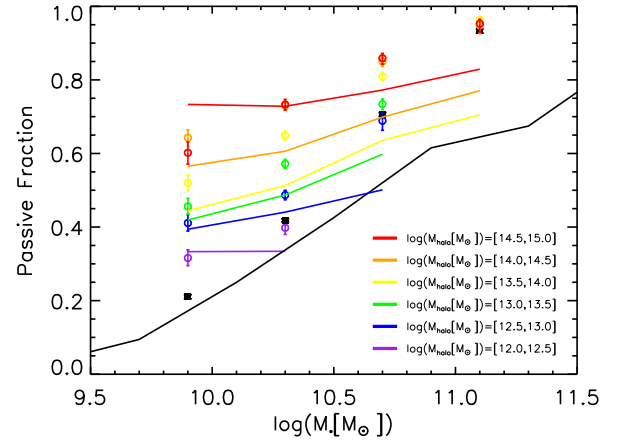


Figure 3. The predicted fraction of passive galaxies as a function of stellar mass (solid lines) compared with observations compiled by Wetzel et al. (2012) (symbols). Black lines and symbols represent the relation for central galaxies while coloured lines and symbols are for satellites in groups of differing mass. Both the observed and model passive galaxies were selected by SSFR ($\log_{10}(\text{SSFR}[\text{yr}^{-1}]) < -11.0$).

ertheless, because the boundary between these two components is ill-defined, different choices emphasize the importance of mergers differently, and can lead to apparent differences at high mass in both observational and simulated stellar mass functions (Bernardi et al. 2013; Kravtsov, Vikhlinin & Meshcheryakov 2014; Schaye et al. 2015).

3.2 The fraction of passive/red galaxies versus stellar mass resulting from AGN quenching

In this subsection we focus on predictions for the fraction of passive galaxies as a function of stellar and halo masses. Our analysis differs from that of red fraction as a function of stellar mass in Paper I, in that we here compare with observational data with better statistics at $z < 1$, we use a bluer colour to classify galaxies ($U - B$ instead of $u - r$), and we separate galaxies according to instantaneous star formation rates, in addition to using colours (the details of the cuts used are presented in Section 2.2). These modifications allow us to compare more closely with the observational analyses of Peng et al. (2010) and Wetzel et al. (2012).

3.2.1 AGN quenching from the fraction of passive galaxies versus stellar mass at $z \approx 0.1$

Fig. 3 shows predictions for the fraction of passive galaxies as a function of stellar mass at $z \approx 0.1$ (solid lines) and compares them with SDSS data compiled by Wetzel et al. (2012). The colours differentiate results for satellite galaxies living in groups/clusters of different mass (for the observations, these masses were estimated by an abundance matching argument rather than measured directly). Black lines and symbols give corresponding results for central galaxies. In the observational samples, the quenched fraction increases both with stellar mass and with halo mass. The latter dependence (together with the fact that satellites of a given stellar mass are more likely to be quenched than centrals) is an environmental effect that we will discuss in more detail in Section 4. Our simulation reproduces these trends quite well, though with some quantitative differences. In particular, the increase in passive fraction with stellar mass for central galaxies is less steep in the

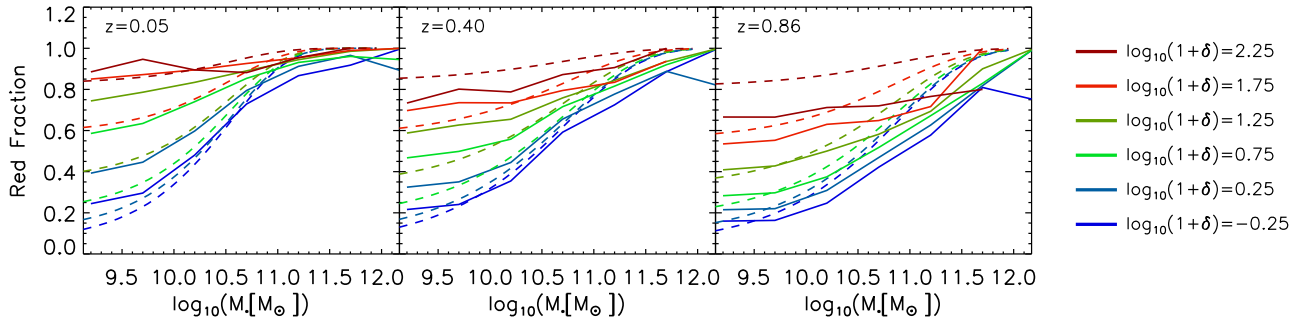


Figure 4. Solid lines show the evolution of the fraction of galaxies predicted to be passive (red) as a function of stellar mass from $z = 0.86$ (right) through $z = 0.4$ (centre) down to $z = 0.05$ (left). Different colours represent different 0.5 dex ranges in density (as inferred from the distance to the fifth nearest neighbour) centred on the values indicated by the labels to the right of the panels. Observational results from SDSS and COSMOS taken from Peng et al. (2010) are shown as dashed lines.

simulation than is observed. Quenching is also somewhat more frequent than observed at low stellar mass and is slightly less complete than observed at high stellar mass.

These discrepancies are larger than found in Paper I. As we confirm in the next subsection, this seems in part to result from using directly estimated SSFRs rather than colours to separate passive from star-forming galaxies. They are also more noticeable in the $U - B$ colours used below than in the $u - r$ colour used in Paper I. This may indicate that although more massive galaxies are dominated by older populations in our model, as observationally required, too many of them still have residual star formation at late times (the same conclusion was recently reached by Luo & Kang 2016). Although we have increased the efficiency of radio-mode feedback at later times, this is not enough to suppress star formation completely. Massive objects that remain star forming at late times are characterized by relatively ‘quiet’ accretion histories, with no major merger below $z = 2$ (these represent ~ 20 per cent of the population at $\log_{10}(M_*[M_\odot]) = 11.0$). This leads to black hole masses below average and little AGN activity and seems to indicate that our model for black hole growth excessively relies on mergers. We checked that the problem is alleviated if we allow black hole growth also in disc instabilities and we will include this modification in future versions of our model.

3.2.2 Evolution of the red fraction as a function of stellar mass

In this subsection we compare our simulation directly to the data which Peng et al. (2010) used to quantify quenching over the redshift range $0 < z \leq 1$. They separated passive galaxies from star-forming galaxies on the basis of rest-frame $U - B$ colour, and then used large observational samples from SDSS and COSMOS to estimate the evolution of quenched fraction as a function of stellar mass. Fig. 4 compares our current model (solid lines) to the fits which Peng et al. (2010) made to their compilation of observations (dashed lines). The different panels refer to different redshifts ($z = 0.05, 0.40$ and 0.86) while the different lines within each panel split the galaxies by environment density (the separation between red and blue galaxies is described in Section 2.2). The proxy for environment density used in the simulation is directly analogous to that used by Peng et al. (2010) and is based on the projected distance to the fifth nearest neighbour with a redshift difference (peculiar velocity + Hubble flow) less than 1000 km s^{-1} . Such distances are calculated for all galaxies with $\log_{10}(M_*[M_\odot]) \geq 9.0$ but only bright neighbours ($M_{B, AB} \leq -19.3 - z$ at $z \leq 0.7$ and $M_{B, AB} \leq -20.5 - z$ at $z > 0.7$) are counted when estimating environment density. The density itself

is given by $\Sigma_{5,i} = 5/\pi d_{5,i}^2$ and the normalized density used in the plots by $1 + \delta_{5,i} = \Sigma_{5,i}/\Sigma_{5,m}$, where $\Sigma_{5,m}$ is the mean density of ‘bright’ galaxies at given redshift.

Model and observations agree qualitatively in the slope of the relations and in their density dependence at all redshifts. In particular, there is a substantial improvement at $z \sim 0$ compared to early attempts at modelling such as that of Baldry et al. (2006). Nevertheless, obvious discrepancies remain at high mass and at high overdensity, for $z > 0.05$, where quenching is less effective than observed (at $z = 0.05$ only the discrepancy at high mass remains). As explained in the previous section, this discrepancy is evident in terms of specific star formation, and it is still noticeable for $U - B$ colours, but it is absent for red galaxies in terms of $u - r$. This indicates that the ages in the model and in the observations are comparable but there is too much ongoing star formation at high mass and environment density in the model, particularly at $z \sim 1$.

While the slopes tell us about AGN/stellar mass quenching efficiency, the different colours indicate the impact of environment. In this case it seems that the model matches observations at the higher redshifts, but overestimates the red fraction in high-density environments at later times (compare solid and dashed lines for each colour at low masses which are not affected by insufficient quenching by AGN feedback). The discrepancy may result from a mismatch in the density calculation or from overly high impact of the environment in the model. This will be analysed in detail in Section 4.

3.3 Evolution of the mass-quenching efficiency

Baldry et al. (2006) and Peng et al. (2010) showed that the mass and environment dependences of the probability that a given galaxy is red (passive) appear to be separable, meaning that the probability can be written as a product of two factors, one depending only on stellar mass and the other depending only on environment density. Analysis in terms of these so-called quenching efficiencies allows us to focus on the impact of AGN feedback and environment independently. Here we compare the observationally inferred evolution of the mass-dependent efficiency to the predictions of our model. Following Peng et al. (2010), the mass-quenching efficiency can be defined as:

$$\varepsilon_m(m, m_0, \rho, z) = \frac{f_{\text{red}}(m, \rho, z) - f_{\text{red}}(m_0, \rho, z)}{1 - f_{\text{red}}(m_0, \rho, z)}, \quad (5)$$

which gives the excess red fraction at stellar mass m relative to the red fraction at the lowest mass considered m_0 for galaxies in environments of density ρ at redshift z . Both observationally and

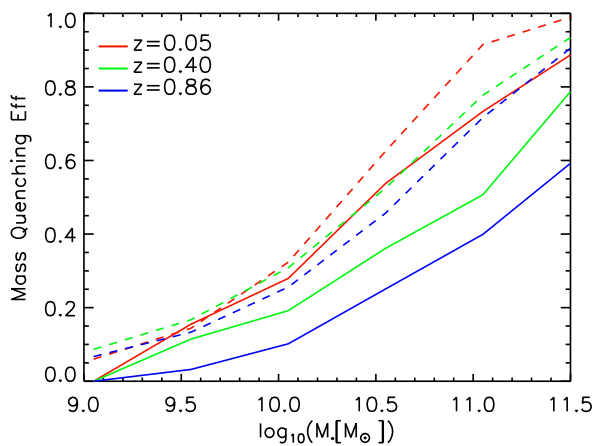


Figure 5. Evolution of the mass-quenching efficiency from $z = 0.86$ to 0.05 . Predictions from our simulation are shown as solid lines, while the fits which Peng et al. (2010) used to represent their compilation of observational data are shown as dashed lines.

in our model, this excess is approximately independent of ρ , so we will present results averaged over environment density.

Fig. 5 compares observational and simulation results for the evolution of environment-averaged mass-quenching efficiency. Solid lines show our model predictions, while dashed lines show fits to observational data from COSMOS and SDSS by Peng et al. (2010). Different colours indicate different redshifts. The trends highlighted in the previous subsection are clearly visible in this plot. The mass-quenching efficiency increases with stellar mass and decreases with redshift over the full range of mass and redshift shown. Overall, the slopes of the model relations are roughly consistent with those observed, indicating that our revised AGN feedback implementation reproduces the observed evolution of the mass-quenching efficiency quite well. In the model, the trends with redshift and stellar mass result from the close but redshift-dependent relations between stellar mass and the properties that control hot gas accretion on to black holes, namely black hole mass and halo hot gas mass. As previously highlighted, a discrepancy remains for the highest masses where AGN feedback is not efficient enough in our model.

3.4 Individual galaxy tracks through the colour-stellar mass diagram

As described above, various quenching mechanisms can move galaxies from the star-forming (blue) to passive (red) population. For example, galaxies may develop a large enough black hole for AGN feedback to prevent cooling of hot gas to replenish their cold interstellar medium, or this medium may be removed by interaction with their environment. Once quenched, ongoing black hole feedback keeps the majority of central galaxies quenched in our models, while further stripping keeps satellites quenched until they merge with the central object of their group/cluster. Nevertheless, it is not uncommon for quenched central galaxies to become star-forming again after major episodes of gas accretion, either from the diffuse intergalactic medium or from merging. AGN feedback is most effective in massive galaxies, making them predominantly red by $z = 0$. It has little effect at low mass, so that dwarf galaxies remain blue unless they are strongly affected by environmental processes.¹

¹ Only ~ 40 per cent of galaxies are satellites at $z = 0$ and only a fraction of those will be quenched.

It is particularly informative to plot the evolution of massive galaxies in a colour-stellar mass diagram, where quenching takes them from being predominantly star-forming at $z > 2$ to predominantly passive at $z = 0$. The stochasticity of black hole and hot gas growth means that AGN feedback quenches different galaxies at different times leading to significantly different tracks in this diagram. Fig. 6 illustrates this; red lines represent the time evolution of individual red massive galaxies in the $(g - r)$ -stellar mass plane ($g - r > 0.6$ and $\log_{10}(M_* [M_\odot]) \geq 11.0$ at $z = 0.1$). In the left-hand panel the median and 16th and 84th percentiles are shown for the evolution of all galaxies (repeated as a dotted black line in the other panels) while the evolution of individual galaxies is plotted in other panels. Coloured dots along these lines mark specific redshifts; black for $z = 3$, blue for $z = 2$, green for $z = 1$ and red for $z = 0.5$. The end of the line corresponds to $z = 0.1$. Overplotted in grey contours is the full galaxy distribution at $z = 0.1$. When comparing the tracks with this distribution, it should be remembered that the corresponding distributions at earlier times were significantly bluer. As described in Section 2.1.1, properties in addition to stellar mass contribute to the impact of AGN feedback on massive galaxies and hence their evolution in this figure. Terrazas et al. (2016b) carry out a detailed analysis of this issue in the context of our model for the particular case of central galaxies in Milky Way mass haloes.

The left-hand panel of Fig. 6 shows the median evolutionary track for massive galaxies. These are star-forming at early times, but quench once their central black hole becomes sufficiently massive. The transition typically happens between redshifts 2 and 1 (the blue and green dots, respectively). Galaxies travel gradually from the blue side to the red side of the star-forming population as they grow in mass, and then move rapidly to the passive population once feedback is able to prevent cooling and accretion of new material and the remaining cold gas is exhausted (seen by the increased steepness of the track below $z = 2$, blue symbol). This results in a broad star-forming sequence and a paucity of galaxies in the ‘green valley’ between the two populations. Once massive galaxies reach the red sequence, the absence of further star-formation and also of minor mergers once they become satellites in groups or clusters causes most systems to grow rather little in mass. It should be noted that the comparative rarity of massive blue galaxies at $z = 0$ is perfectly compatible with this path. There were more such galaxies at $z = 2$, but most have now become passive, a sequence often referred to as ‘down-sizing’ of star-formation activity.

The left middle panel of Fig. 6 shows a less common, but still significant, evolutionary pathway in which galaxies quench early and then grow substantially through mergers: galaxies which become red at $z \geq 2$ (5.0 per cent of all galaxies with $g - r > 0.6$ and $\log_{10}(M_* [M_\odot]) \geq 11.0$ and 17.0 per cent of all galaxies with $g - r > 0.6$ and $\log_{10}(M_* [M_\odot]) \geq 11.5$ at $z = 0.1$). Such massive galaxies begin life as the central objects of high-mass haloes that undergo early gas-rich mergers, resulting in substantial black hole growth. This can produce enough AGN feedback at this early stage to quench star formation entirely. Later growth then occurs through accretion of satellite galaxies on to the central object of the group/cluster. Another extreme case, this time of early mass-assembly, is shown in the middle right panel: galaxies which have increased their mass by less than a factor of 2 since $z = 2$ (10.6 per cent of all galaxies with $g - r > 0.6$ and $\log_{10}(M_* [M_\odot]) \geq 11.0$ and 21.6 per cent of all galaxies with $g - r > 0.6$ and $\log_{10}(M_* [M_\odot]) \geq 11.5$ at $z = 0.1$). One of these galaxies is already as massive as $10^{11.5} M_\odot$ at $z = 3$ (right most black dot). While such early growth of massive objects may seem ‘anti-hierarchical’, it is clearly fully compatible with Λ CDM

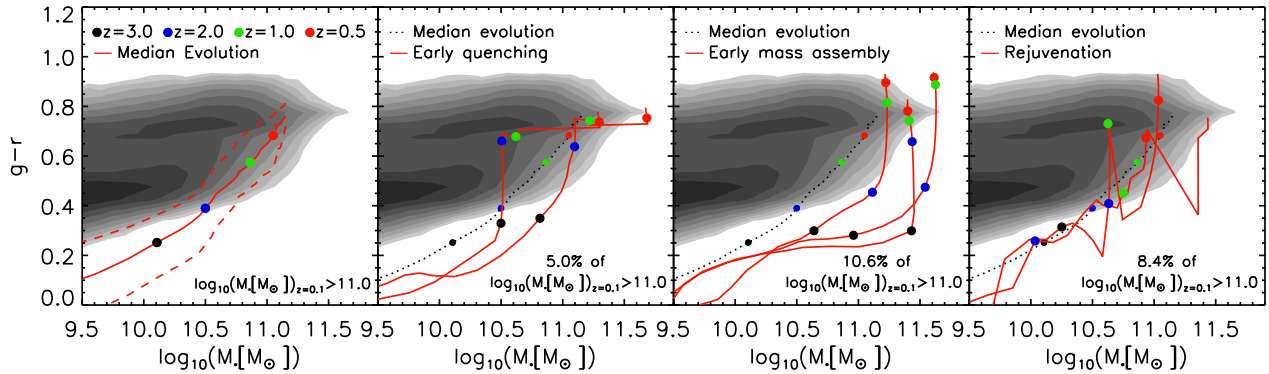


Figure 6. Evolutionary tracks of quenched galaxies with $\log_{10}(M_* [M_\odot]) \geq 11.0$ at $z = 0.1$ in the $g - r$ versus stellar mass plane (solid red lines). In the left-hand panel, the median and 16th and 84th percentiles are shown for the evolution of all galaxies (repeated as a dotted black line in the other panels) while the evolution of individual galaxies is plotted in other panels. Various redshifts are marked with filled circles of differing colour.

structure formation once baryonic physics are taken into account. Finally, the right-hand panel of Fig. 6 shows examples of galaxies that return to the blue population after being quenched: galaxies which have decreased their ($g - r$) colour by more than 0.1 after reaching the red population ($(g - r) = 0.6$) (8.4 per cent of all galaxies with $g - r > 0.6$ and $\log_{10}(M_* [M_\odot]) \geq 11.0$ and 10.2 per cent of all galaxies with $g - r > 0.6$ and $\log_{10}(M_* [M_\odot]) \geq 11.5$ at $z = 0.1$). This is normally a consequence of direct accretion of cold gas from satellites. Since such galaxies contain a massive black hole that previously shut down cooling, the return to the passive population tends to be quick. The fraction of rejuvenated galaxies is significantly higher in star-formation rate than in colour (22 per cent of all galaxies with $\log_{10}(\text{SSFR}[\text{yr}^{-1}]) < -11$ and $\log_{10}(M_* [M_\odot]) \geq 11.0$ at $z = 0.1$). Any short star formation episode can move a galaxy from the passive to the star-forming population but a predominantly blue population is required to move it from the red to blue cloud. However, at any given epoch, rejuvenated galaxies never represent more than 1 per cent of the star-forming population and are not the cause for the ~ 20 per cent massive star-forming galaxies in our model. As previously explained, this is the result of having a black hole growth model that excessively depends on mergers.

4 ENVIRONMENTAL QUENCHING

In this and subsequent sections, we will focus on environmental quenching, an effect caused in our model by the removal of gas from satellite galaxies as they orbit within the halo of a larger system. As in the previous section, we will consider the fraction of galaxies of given stellar mass which are passive or red, but now as a function of environment rather than of stellar mass. In this section, we will study quenched fractions as a function of host halo mass, of distance to group centre, and of local number density of galaxies. In Section 5, we will study how environmental quenching affects the mass- and colour-dependent autocorrelation functions of galaxies. Finally, in Section 6, we will look at how the combined effects of AGN and environment result in the observed conformity between the properties of central and satellite galaxies. We emphasize that despite ram-pressure stripping being switched off in low-mass groups in our current model, satellites still experience strong environmental effects as a result of both of the suppression of primordial infall and of tidal stripping by the group potential.

4.1 Passive fraction versus halo mass

Fig. 7 shows SSFR distributions for satellite galaxies in various bins of stellar mass and group/cluster mass. From left to right, the panels give results for galaxies of increasing stellar mass, as indicated by the legend. Within each panel, different coloured lines correspond to different group masses as indicated by the key at bottom left. The top row shows results for the model of Guo et al. (2013), the middle row for the model of this paper, and the bottom row for SDSS data as compiled by Wetzel et al. (2012). All distributions have been normalized to enclose the same area. In the models, the halo mass is obtained directly from the dark matter simulation, after scaling to the appropriate cosmology. For the SDSS data, an abundance matching approach was taken to assign sets of central+satellite galaxies to haloes of differing mass. As explained in Paper I, in order to match the observed distribution of unclassified galaxies with no emission lines, that were assigned a value of SFR based on SED fitting, model galaxies with $\log_{10}(\text{SSFR}[\text{yr}^{-1}]) < -12$ have been assigned a random Gaussian value centred at $\log_{10}(\text{SSFR}[\text{yr}^{-1}]) = -0.3 \log_{10}(M_* [M_\odot]) - 8.6$ and with dispersion 0.5.

Some clear trends can be identified in the observational data (bottom row of Fig. 7). Massive galaxies are predominantly passive, irrespective of the mass of the group they reside in (lines of all colours peak at low SSFR in the bottom right-most panel). Conversely, in the high-mass clusters, galaxies are predominantly passive, irrespective of their stellar mass (the red lines peak at low SSFR in all three panels of the bottom row). For intermediate mass galaxies, the passive fraction increases strongly with increasing halo mass (middle panels of the bottom row).

These trends are reproduced qualitatively by our model (the middle row in Fig. 7). Galaxies in higher mass groups/clusters, even those with lower stellar and black hole masses, suffer stronger environmental effects and are more likely to be quenched. This trend extends down to low-mass groups, where ram-pressure stripping is switched off, because other environmental processes are still active. In fact, environmental effects are stronger in our new model than in Guo et al. (2013), as can be seen from the larger passive peaks (at $\log_{10}(\text{SSFR}[\text{yr}^{-1}]) \sim -12$) for galaxies with $\log_{10}(M_* [M_\odot]) > 9.4$ (compare the top and middle rows in the three rightmost panels). This is caused by the more efficient supernova feedback introduced by Henriques et al. (2013), which suppresses the early formation of low-mass galaxies, balancing it with re-incorporation and primordial infall at later times. Since none of the replenishing channels are available for satellites, the stronger feedback results in quicker

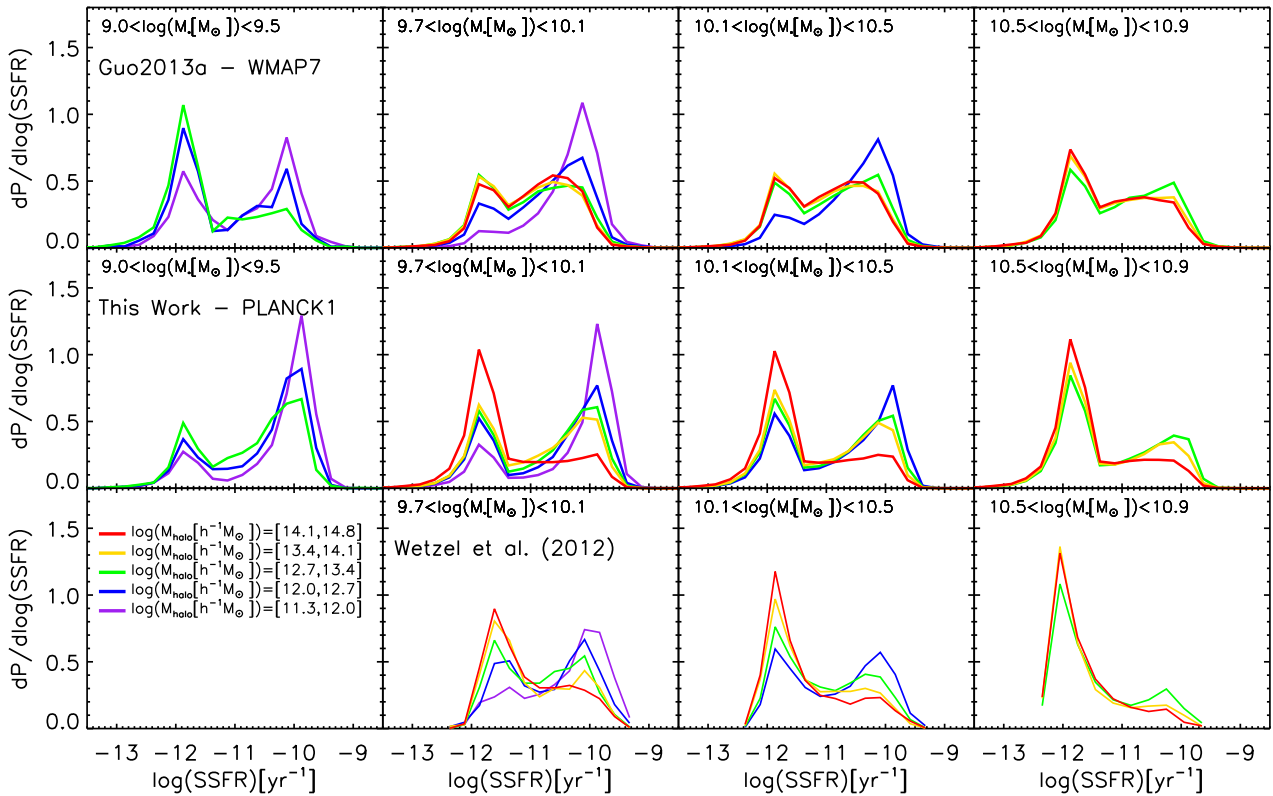


Figure 7. SSFR histograms for different halo masses (different colours) and for different stellar mass bins (low stellar mass left-hand panels, high stellar mass right-hand panels). The top row shows predictions from Guo et al. (2013), the middle row shows predictions from the model of this paper, while the bottom row shows observational results compiled by Wetzel et al. (2012).

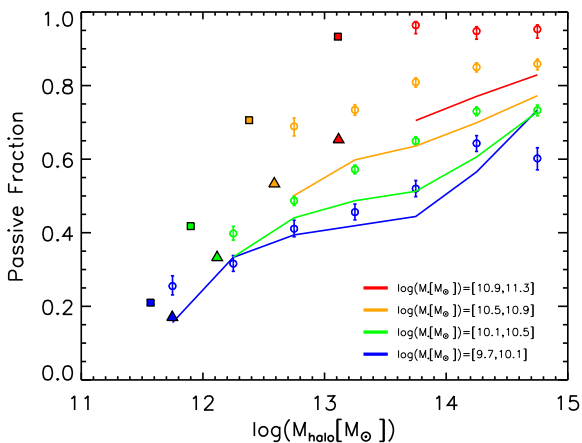


Figure 8. The fraction of satellite galaxies that are passive as a function of host halo mass (defined as those with $\log_{10}(\text{SSFR}[\text{yr}^{-1}]) < -11$). Solid lines and open circles represent model predictions and observational data from SDSS (again from Wetzel et al. 2012), respectively. Different colours refer to galaxies of different stellar mass as indicated in the legend. Filled triangles and filled squares indicate the passive fraction and mean halo mass of *central* galaxies with the corresponding stellar mass in our models and in the SDSS respectively.

depletion of gas in such objects. The impact of the weaker ram-pressure stripping and the lower threshold for star formation is evident only for the lowest mass galaxies, resulting in a smaller passive peak (left-hand panel, for $8.7 < \log_{10}(M_*[M_{\odot}]) < 9.2$).

A simpler version of the same data is shown in Fig. 8, where the passive fraction of satellite galaxies (defined as those with

$\log_{10}(\text{SSFR}[\text{yr}^{-1}]) < -11$) is plotted as a function of group/cluster mass, with different colours representing different stellar mass ranges. The circles with error bars are SDSS data taken from Wetzel et al. (2012), while the solid lines are predictions from our model. Filled triangles and squares mark the passive fraction and mean halo mass of *central* galaxies with the corresponding stellar mass in our model and in the SDSS, respectively. As seen in the previous figure, our model is roughly consistent with observation. The variation in passive fraction with host halo mass (i.e. the slope of the relation) agrees well, but there is a discrepancy in normalization at high stellar mass which, as discussed in previous sections, reflects the fact that, even with our more efficient AGN feedback, massive galaxies still seem to have too much ongoing star formation at late times. This is also seen clearly in the offset between model and observation in the passive fraction of central galaxies.

4.2 Passive fraction versus distance to group centre

A different test of our implementation of environmental effects comes from looking at how the fraction of satellite galaxies that are passive varies with distance from group centre. Although individual orbits can span a wide range of radii, satellites seen closer to group centre have, on average, spent more time as group members and have spent that time in denser regions. Thus, they are more likely to be environmentally quenched, and the radial dependence of passive satellite fractions should be sensitive both to the variation of the strength of environmental effects with radius and to the time-scale on which star formation is suppressed.

Fig. 9 shows the fraction of passive galaxies as a function of projected radius for different ranges of halo/group mass (top

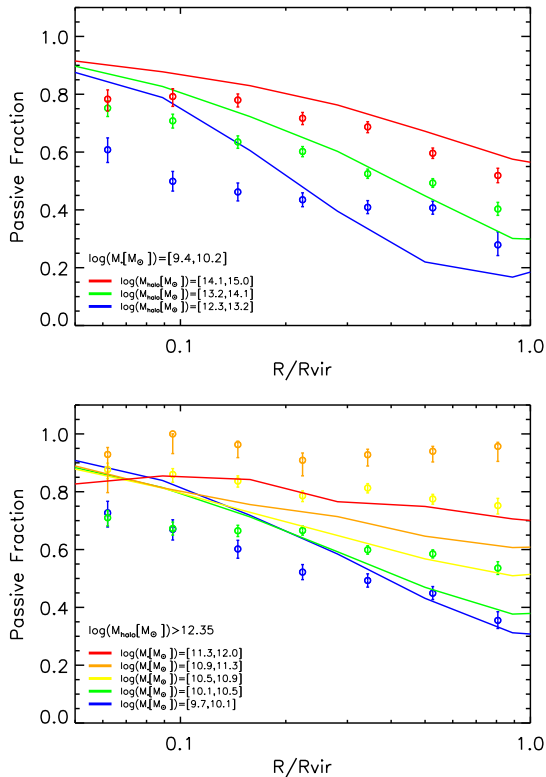


Figure 9. The fraction of passive galaxies (defined as those with $\log_{10}(\text{SSFR}[\text{yr}^{-1}]) < -11$) as a function of projected distance from the central galaxy in bins of group mass (top) and (satellite) stellar mass (bottom). Model predictions are shown as colored lines and SDSS data from Wetzel et al. (2012) as coloured symbols.

panel) and also for different ranges of galactic stellar mass (bottom panel). In the first case, all curves refer to galaxies with $9.4 \leq \log_{10}(M_*[M_\odot]) \leq 10.2$, while in the second, all curves are for galaxies in groups with $\log_{10}(M_{\text{vir}}[M_\odot]) > 12.35$. Over the range $0.3 < R/R_{\text{vir}} < 1$, the model agrees well with the SDSS data compiled by Wetzel et al. (2012) (top panel and low stellar masses in the bottom panel). This is consistent with results shown in previous sections where similar agreement was found for the population of satellites as a whole in different stellar masses and halo mass bins. Nevertheless, it seems clear from both panels that the model relations are steeper than observed, resulting in too many passive galaxies near group centre. This is particularly clear for low-mass satellites and in low-mass groups. We emphasize that this is a subdominant population, since most satellites orbit at large radii. This explains why such discrepancies were not evident in the global trends. In addition, it is once again clear in the bottom panel that massive galaxies have too much ongoing star-formation. This is seen at all radii and reflects the inability of our AGN feedback model to quench all of these galaxies in the field.

Fig. 10 shows the cumulative quenched fraction ($\log_{10}(\text{SSFR}[\text{yr}^{-1}]) < -11$) as a function of time since infall for $z = 0$ galaxies that became satellites at $z \sim 1$. For the various satellite and host halo masses considered, the time at which most satellites become quenched varies very little ($\sim 2 - 4$ Gyr). This is consistent with observational estimates, $\sim 2 - 5$ Gyr (McGee et al. 2009; McGee, Bower & Balogh 2014; Wetzel et al. 2013), although these seem to favour a ‘delayed-then-rapid’ quenching rather than our steady increase in quenched fraction. Even though, in our current model, ram-pressure stripping acts only in groups

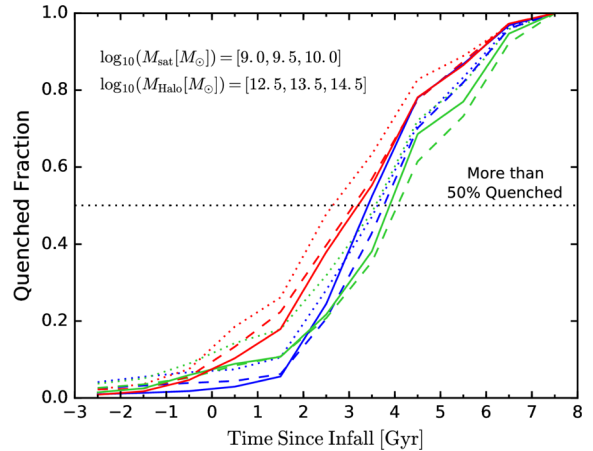


Figure 10. Cumulative quenched fraction $\log_{10}(\text{SSFR}[\text{yr}^{-1}]) < -11$ as a function of time since infall for $z = 0$ galaxies that became satellites at $z \sim 1$. Different colours represent different host halo mass (blue: $\log_{10}(M_{\text{vir}}[M_\odot]) = 12.5$, green: $\log_{10}(M_{\text{vir}}[M_\odot]) = 13.5$, red: $\log_{10}(M_{\text{vir}}[M_\odot]) = 14.5$) while different line styles correspond to different satellite masses (dotted: $\log_{10}(M_{\text{sat}}[M_\odot]) = 9.0$, dashed: $\log_{10}(M_{\text{sat}}[M_\odot]) = 9.5$, solid: $\log_{10}(M_{\text{sat}}[M_\odot]) = 10$).

with $\log_{10}(M_{\text{vir}}[M_\odot]) > 14.0$, it seems that the lack of primordial infall or other gaseous accretion on to satellites combines with the expulsion of ISM by supernova feedback and the removal of hot gas by tidal stripping to produce quenching, on average, on the right time-scale. The excess of low mass red galaxies near the centre of groups apparently arises not from overly short quenching time-scales, but rather from overly strong environmental effects in that region. Despite the significant modelling improvements introduced recently to address problems pointed out by Font et al. (2008), Weinmann et al. (2010) and Guo et al. (2011) among others, these remaining discrepancies show that further modifications are needed. A possibility might be to include interaction-induced star formation as suggested by Wang et al. (2014).

It should be noted that in building the observed group catalog, it was assumed that the most massive galaxy is always at the centre. This is not necessarily the case in the model, which can, in principle, lead to artificial discrepancies between theory and observations. However, our halo finder assumes that the group centre is given by that of the most massive subhalo and the tight relation between subhalo and galaxy properties means that the most massive galaxy will normally be in the centre. This is the case for over 95 per cent of haloes with $\log_{10}(M_{\text{vir}}[M_\odot]) > 12.0$.

4.3 Evolution of the relation between red fraction and environment density

In order to compare with the SDSS and COSMOS data compiled by Peng et al. (2010), we now use distance to the fifth nearest neighbour galaxy as an indicator of environment and study how it affects the quenching of galaxies as indicated by their rest-frame $U - B$ colours (the separation between red and blue galaxies is described in Section 2.2). This allows us to test our model against observations up to $z \sim 1$, providing significant constraints on how well it represents the time evolution of environmental effects. Details of the density calculations are described in Section 3.2.2.

Fig. 11 compares our model (solid lines) to the fits which Peng et al. (2010) used to represent the dependence of red fraction on environment density which they infer from their compilation of

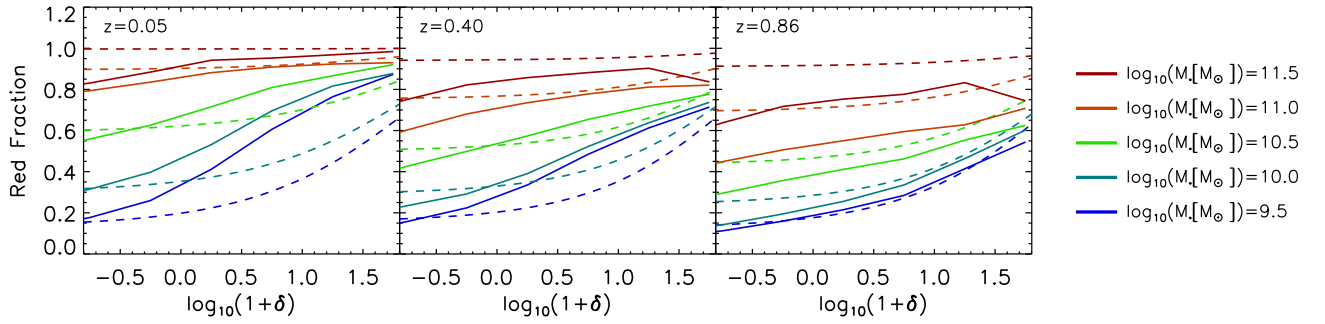


Figure 11. The predicted evolution of the fraction of red galaxies as a function of local galaxy density as measured by the distance to the fifth nearest neighbour (solid lines) from $z = 0.86$ (right-hand panel), to $z = 0.40$ (middle panel) to $z = 0.05$ (left-hand panel). The different colours represent different bins of stellar mass as indicated. Fits by Peng et al. (2010) to their compilation of SDSS and COSMOS observations are shown as dashed lines.

SDSS and COSMOS data (dashed lines); different colours show results for different stellar mass ranges. The left-hand, middle and right-hand panels are for galaxy samples with mean redshift, 0.05, 0.40 and 0.86, respectively. At high redshift (the right-hand panel), the model agrees quite well with observation, matching the increase in red fraction from low to high density at all stellar masses (compare the slopes of the solid and dashed lines). At later times, the model relations seem too steep, producing excessive red fractions at moderate to large overdensities. This is another reflection of the overly strong quenching in the central regions of groups and clusters pointed out in the previous section. It is interesting that overly strong quenching is seen only at $z < 0.5$.

In order to separate environmental from AGN quenching in a complementary way to that of Section 3.3, we again follow Peng et al. (2010) and define a redshift-dependent environmental-quenching efficiency as the excess red galaxy fraction at each environment density with respect to that at the lowest density:

$$\varepsilon_\rho(\rho, \rho_0, m) = \frac{f_{\text{red}}(\rho, m) - f_{\text{red}}(\rho_0, m)}{f_{\text{blue}}(\rho_0, m)}. \quad (6)$$

As explained in Section 3.3, AGN and environmental quenching are, to a good approximation, separable, meaning that the efficiency defined by this equation is at most weakly dependent on stellar mass. We therefore present results for $\varepsilon_\rho(\rho, \rho_0)$ averaged over stellar mass.

Fig. 12 compares our model’s prediction for this quantity (solid lines) to the analytic fit which Peng et al. (2010) use to represent their observational data (dashed lines). Blue, green and red lines represent redshifts 0.86, 0.40 and 0.05, respectively. As expected from Fig. 11, model and observations agree reasonably well at $z = 0.86$ (except at the highest densities), but at lower redshifts, the environmental quenching efficiency in the model seems higher than observed (see also the end of Section 4.2). Despite the considerable improvements achieved with our model updates, this again indicates that environmental processes remain too strong, particularly in the inner regions of groups and clusters. With respect to the highest overdensities (right-most values), it seems that our model has the correct environmental quenching efficiency by $z = 0.05$ but decreases more than observed at higher redshifts. A recent study suggests that such evolution may be present at even higher redshifts ($z > 0.9$), with quenching efficiencies dropping to 0.2 by $z = 1.6$ (Nantais et al. 2016). A similar result is presented in the work of Darvish et al. (2016), who find similar quenched fractions in higher densities environments from $z = 0$ to $z = 1$ but little relation between quenching efficiency and environment at higher redshifts.

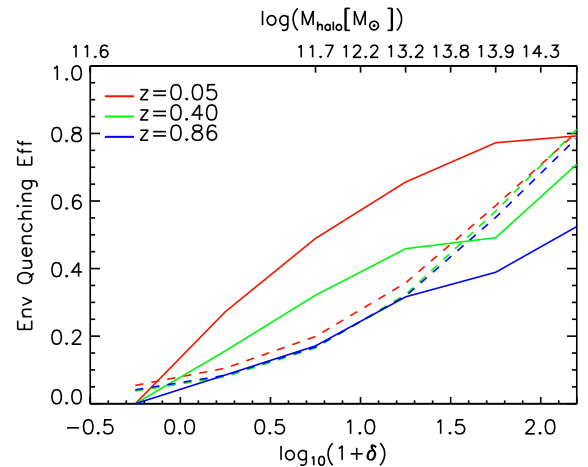


Figure 12. Evolution of the environmental quenching efficiency from $z = 0.86$ –0.1. Predictions from our model are shown as solid lines while those of the fitting function which Peng et al. (2010) used to represent their SDSS and COSMOS observations are shown as dashed lines. The top x -axis shows the median halo mass at each density.

5 GALAXY CLUSTERING

Galaxy clustering can be measured relatively precisely and in considerable detail using two-point auto- and cross-correlations as a function of scale, redshift and galaxy properties (e.g. Li et al. 2006; Zehavi et al. 2011; Mostek et al. 2013). These provide a stringent test of whether galaxy formation models form the right galaxies in the right places and at the right times. They are of particular interest for our current study, since small-scale correlations are very sensitive to how galaxies populate dark matter haloes, and so to the environmental processes which are our primary concern. These produce systematic differences between central and satellite galaxies, as well as systematic variations of satellite properties with halo mass and halocentric radius.

In principle, clustering is also sensitive to the parameters of the background cosmological model, since these determine the abundance and clustering of dark matter haloes (e.g. Mo & White 2002). Guo et al. (2013) showed that the parameter shifts from *WMAP1* to *WMAP7* result in rather small shifts in the abundance and clustering of haloes which can easily be compensated by small changes in galaxy formation parameters. As shown in Paper I, the move to a *Planck* cosmology brings dark halo properties even closer to those in the original *WMAP1* cosmology of the Millennium Simulations. As a result, any difference in clustering between the model

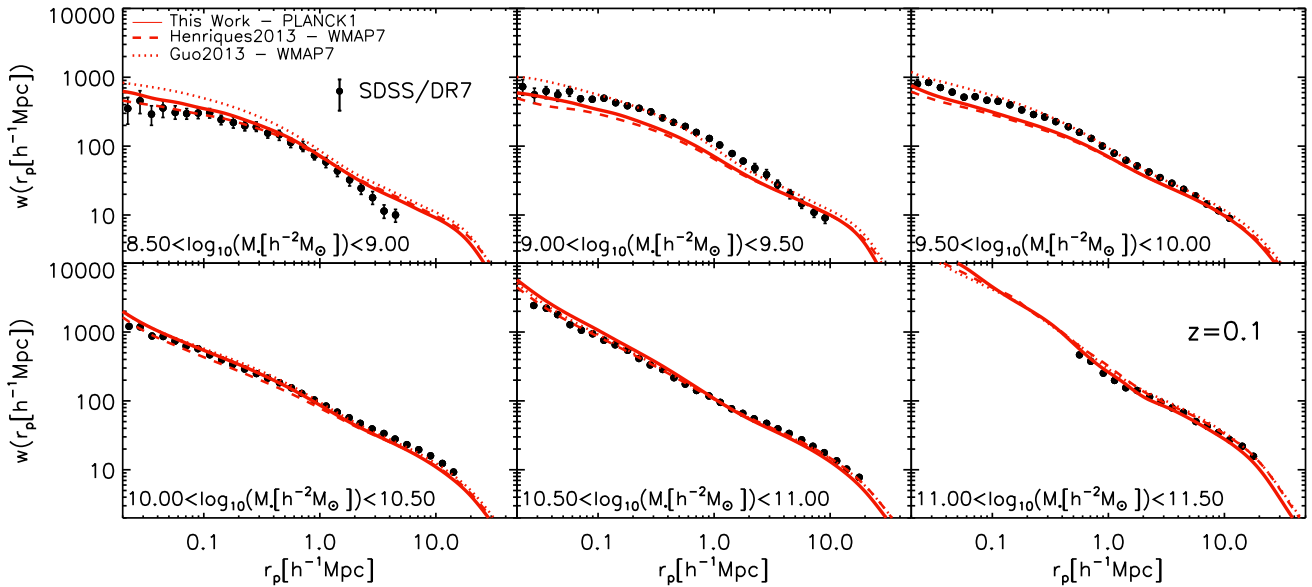


Figure 13. Projected two-point autocorrelation functions for galaxies in six disjoint stellar mass ranges at $z = 0.1$. Results from our new model with its best-fitting parameter values (solid red lines) are compared with model results from Henriques et al. (2013) (dashed red lines) and Guo et al. (2011) (dotted red lines) and observational results based on SDSS/DR7 (black symbols, taken from Guo et al. 2011).

of this paper and that of Guo et al. (2011) is likely a consequence of changes in astrophysical modelling, rather than of changes in cosmology. Indeed, Henriques et al. (2013) found that changes in the strength of feedback and in the reincorporation time for ejected gas produce larger changes in how low-mass galaxies populate massive haloes than any of the cosmological parameter shifts they considered. Here we will further test the impact of our modified physical modelling and of adopting a *Planck* cosmology, and we will extend the analysis to $z = 1$. We will also study clustering differences between active and passive galaxies. These directly reflect the nature of the quenching processes which concern us.

5.1 Projected autocorrelations as a function of stellar mass at low redshift

In Fig. 13 we plot projected autocorrelation functions for galaxies in a series of disjoint stellar mass ranges. Predictions from the models of this paper (solid red lines), of Henriques et al. (2013) (dashed red lines) and of Guo et al. (2013) (dotted red lines) are compared with SDSS/DR7 results taken from Guo et al. (2011). The first and second models differ primarily in cosmology, the second and third only in galaxy formation modelling. As already discussed in Henriques et al. (2013), the most significant differences between the Guo et al. (2013) model and the other two are the enhanced supernova feedback strength and the altered scaling of the gas reincorporation time. As a result, low-mass galaxies are significantly less clustered both in Henriques et al. (2013) and in our new model than in Guo et al. (2013). This reduction is slightly compensated by the particular best-fitting parameter choice adopted in the new model, resulting in somewhat better agreement with observation for $9.0 < \log_{10}(M_* [h^{-2} M_{\odot}]) < 10.0$. Nevertheless, Guo et al. (2013) (and indeed also Guo et al. 2011) still reproduce observed low-redshift clustering better than our more recent models in this mass interval. This emphasizes the need to use clustering observations directly as additional constraints in future MCMC analyses if these are to exploit fully the information content of modern surveys (see van Daalen et al. 2016, for a first attempt). The weak impact of

cosmology is evident in the agreement of the present model with Henriques et al. (2013) on small scales and in the agreement of all three models on large scales. This reflects the very small shifts in cosmological parameters (and hence in structure growth) allowed by modern CMB data.

5.2 Projected autocorrelations as a function of stellar mass at $z \sim 1$

Having compared clustering predictions for our new model with low-redshift observations, we now repeat the exercise at $z \sim 1$, the earliest time for which there are detailed measurements. This provides further insight into whether galaxies are correctly populating the growing dark halo distribution. In Fig. 14, we compare projected autocorrelation functions for our current model (solid red lines) and for those of Henriques et al. (2013) (dashed red lines) and Guo et al. (2013) (dotted red lines) with two observational analyses of the DEEP2 survey, green-filled circles from Mostek et al. (2013) and black-filled circles from Li et al. (2012).

The similarity between the three models is striking, holding over factors of 300 in stellar mass and 1000 in radius. While the difference in the treatment of low-mass galaxies between Guo et al. (2013) and the two more recent models results in different clustering strengths at $z \sim 0$, the three models make almost identical clustering predictions at $z = 1$, despite the fact that the predicted abundance of low-mass galaxies is significantly reduced at this redshift in the newer models (see Henriques et al. 2013, and Paper I). There is also remarkable agreement both at low redshift and at $z \sim 1$ between the results of Henriques et al. (2013) in the *WMAP7* cosmology and our new model in its *Planck* cosmology. As noted by Guo et al. (2013), although there are small differences in the growth of structure in the two cosmologies, these are not visible in galaxy clustering once the physical parameters have been re-adjusted to match the stellar mass function at the relevant times. Finally, all models predict clustering at $z \sim 1$, which appears slightly stronger than observed, particularly for $\log_{10}(M_* [h^{-2} M_{\odot}]) < 10.19$ and on small scales. This may reflect problems with the model's treatment of satellite dynamics or

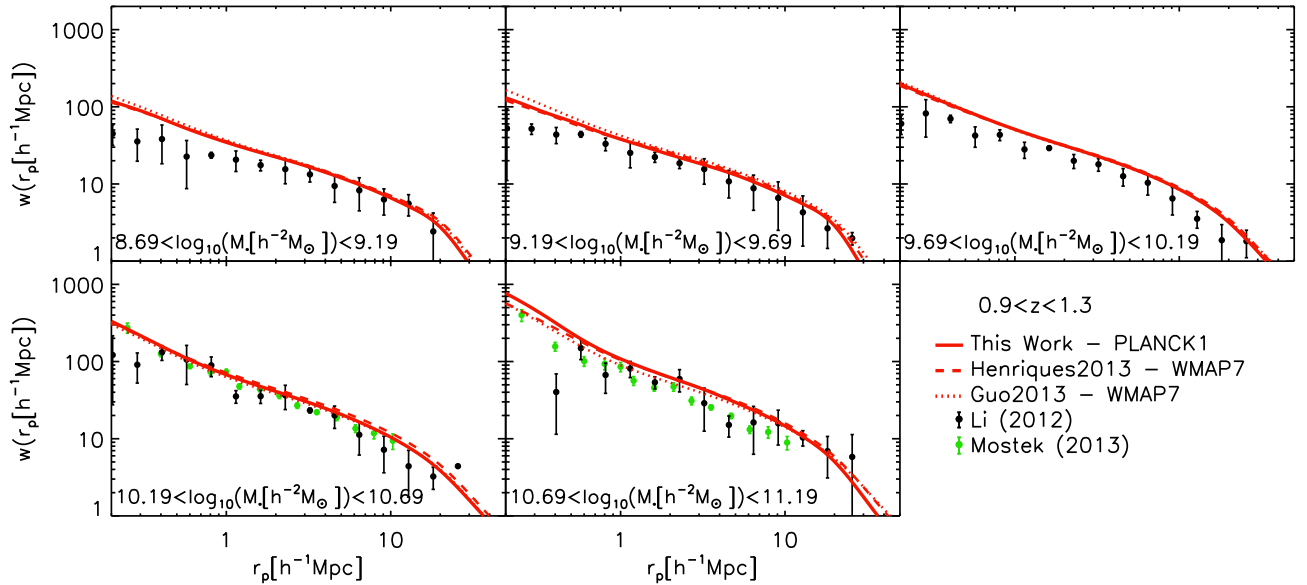


Figure 14. Projected two-point autocorrelations for galaxies in five disjoint stellar mass ranges at $z \sim 1$. Results from our new model with its best-fitting parameter values (solid red lines) are compared with model results from Henriques et al. (2013) (dashed red lines) and Guo et al. (2011) (dotted red lines) and with observational results from DEEP2 (black and green symbols taken from Li et al. 2012 and Mostek et al. 2013, respectively). The Millennium-II Simulation is used for $\log_{10}(M_* [M_\odot]) \leq 9.5$ and the Millennium Simulation for higher stellar masses.

in our rough approximation to the completeness corrections and selection functions used when analysing the observational data.

5.3 Low-redshift projected autocorrelations as a function of stellar mass and colour

In this subsection we compare our new model to observations of the low-redshift clustering of galaxies split by colour into star-forming and passive populations (the separation between red and blue galaxies is described in Section 2.2). The difference in clustering between red and blue galaxies is very sensitive to the physics of quenching which is the main concern of this paper. Quenching by environment will turn satellite galaxies red, particularly in massive haloes where ram-pressure stripping is effective, but does not depend strongly on the mass of the satellite. Radio-mode AGN quenching, on the other hand, primarily affects the central galaxies of relatively massive haloes, which themselves have relatively high stellar mass.

On large scales, galaxy autocorrelations are due to galaxy pairs which reside in different haloes and, except at relatively small stellar mass, are dominated by pairs in which both galaxies are centrals. As a result, the colour dependence of autocorrelation strength at given stellar mass arises partly because red centrals live in more massive haloes than blue ones (e.g. Mandelbaum et al. 2016, and references therein) and partly because the (subdominant) fraction of pairs where at least one galaxy is a satellite (and hence typically lives in a substantially more massive halo) is larger for red galaxies than for blue ones.

In contrast, small-scale galaxy autocorrelations are dominated by pairs in which both galaxies reside in the same halo, so that at least one of them is a satellite. For low-mass galaxies, both galaxies are satellites in the majority of close pairs. As a result, small-scale autocorrelations as a function of colour are very sensitive to environmental quenching.

In Fig. 15, the red and blue symbols give autocorrelation functions estimated separately from the SDSS/DR7 main galaxy sample for active and passive galaxy samples split according to the above

colour cut. Results are shown for six disjoint ranges in stellar mass spanning a total range of a factor of 1000. In the two lowest stellar mass bins the total volume surveyed is relatively small and the error bars underestimate the uncertainties which are dominated by cosmic variance. This primarily affects the large-scale clustering. The curves in each panel give predictions for the same three models as in Figs 13 and 14.

The variation with colour of these autocorrelation functions is large, both for the observations and for the models. The difference in behaviour between the one- and two-halo terms is also very clear, particularly for the lower stellar masses, where the amplitude of the one-halo term is well over an order of magnitude higher for red galaxies than for blue galaxies. On a large scale, the red to blue difference is still substantial (of order a factor of 2) except for the highest stellar masses, where there are very few blue galaxies.

Given the very large dynamic range in both stellar mass and projected radius which is plotted here, the models agree remarkably well (although not perfectly) with the SDSS data, suggesting that the interplay of internal and environmental effects is being relatively well captured as a function of stellar mass. Further improvement will require a more rigorous characterization of the uncertainties in the observed autocorrelations, and the use of the clustering measurements as additional constraints in the MCMC exploration of model parameter space (e.g. by extending the methods in van Daalen et al. 2016).

6 CONFORMITY

In previous sections, we explored how well the observed trends of quenching with stellar mass and environment are reproduced by our new model. Although treated as separate processes, AGN quenching and environmental quenching are clearly connected in the model. Hot gas masses are larger in more massive haloes, leading to enhanced black hole accretion and AGN feedback in denser environments. In addition, such environments promote black hole growth by enhancing both mergers with smaller black holes and

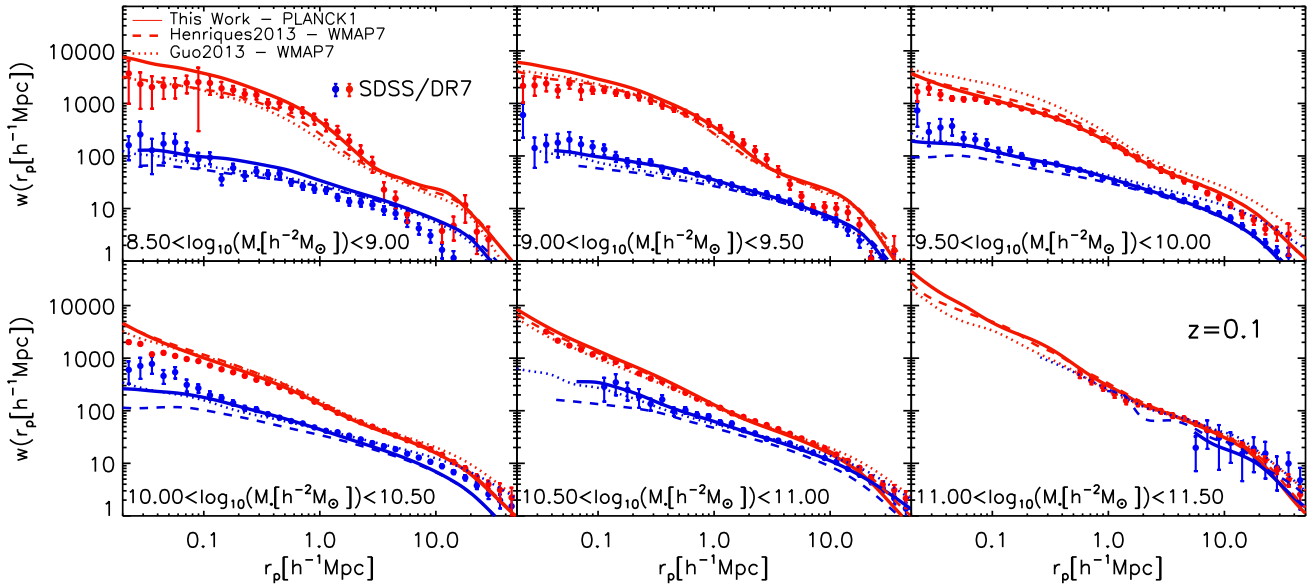


Figure 15. Projected two-point autocorrelations for galaxies in six disjoint stellar mass ranges at $z = 0.1$ and for blue and red galaxies separated according to rest-frame $g - r$ colour. Results from our new model with its best-fitting parameter values (solid lines) are compared with model results from Henriques et al. (2013) (dashed lines) and Guo et al. (2011) (dotted lines) and with observational results from SDSS/DR7 (symbols, taken from Guo et al. 2011). Red and blue colours correspond to the passive and active galaxy populations, respectively. The Millennium-II Simulation is used for $\log_{10}(M_* [M_{\odot}]) \leq 9.5$ and the Millennium Simulation for higher stellar masses.

merger-stimulated accretion of cold gas. At the same time, larger halo and hot gas masses boost environmental quenching through tidal and ram-pressure stripping. As a result, one may expect that quenched central galaxies will typically have more massive haloes and more massive hot gas atmospheres than blue centrals of similar stellar mass, and that this will cause a larger fraction of their satellites to be quenched. Wang & White (2012) showed that this effect is indeed present in the Guo et al. (2011) model and compared its strength to the effects they found in SDSS data, demonstrating that all the observed trends with satellite and primary stellar mass are reproduced qualitatively by the model but that its satellites are systematically too red.

The effect that passive centrals tend to have passive satellites and vice versa was first noticed in SDSS groups by Weinmann et al. (2006), who designated it ‘galactic conformity’. A number of studies have confirmed the strength of this tendency and investigated its variation with primary and satellite properties, with halo mass, with halocentric distance and with redshift (Ann, Park & Choi 2008; Kauffmann et al. 2010; Prescott et al. 2011; Wang & White 2012; Kauffmann et al. 2013; Phillips et al. 2014; Hartley et al. 2015; Knobel et al. 2015). By counting satellite candidates to $r = 21$ in the SDSS/DR8 photometric catalogues around isolated central galaxies brighter than $r = 16.7$, Wang & White (2012) were able to measure conformity over a wide range of primary and satellite stellar masses and we shall compare our current model to their data in this section. We therefore define model primaries in a manner which closely reflects their observational criteria.

Specifically, we select isolated galaxies as those for which every companion projected at $r_p < 0.5$ Mpc and with redshift difference $|\Delta z| < 1000 \text{ km s}^{-1}$ is at least a magnitude fainter in the SDSS r band, and for which no companion within $r_p < 1.0$ Mpc and $|\Delta z| < 1000 \text{ km s}^{-1}$ is brighter. The simulation boxes are projected in three orthogonal directions, parallel to their x -, y and z -axes, and redshifts are assigned based on the ‘line-of-sight distance’ and peculiar velocity of a galaxy. For a set of primaries, defined as

isolated galaxies with stellar mass and colour lying in predetermined ranges, we then identify the set of potential satellites as all objects at least a magnitude fainter than, and projected within 300 kpc of, some primary. This set will include foreground and background objects unassociated with the primaries. We correct for these using the mean surface density of galaxies as a function of absolute magnitude and colour for the simulation as a whole (see Wang & White 2012 for details).

Fig. 16 shows the comparison of SDSS observational results to the model of Guo et al. (2011) that was already presented in Wang & White (2012) (their figs 12 and 13), while Fig. 17 is identical except that the data are now compared with our new model. In each panel, coloured symbols show the cumulative distribution of $^{0.1}(g - r)$ colour for SDSS satellites, with error bars derived by boot-strap resampling of the primary sample, while the coloured curves refer to the models and have negligible statistical uncertainty. In order to have a fair comparison with observations, model colours at $z = 0$ are converted to $^{0.1}(g - r)$ using the relations from Blanton & Roweis (2007): $^{0.1}g = g + 0.3113 + 0.4620 \times ((g - r) - 0.6102)$ and $^{0.1}r = g - 0.4075 - 0.8577 \times ((g - r) - 0.6102)$. Each colour corresponds to a disjoint primary stellar mass range, as indicated in the legend. The two columns of panels refer to the two disjoint ranges of satellite stellar mass indicated by labels above each column. The three rows refer, respectively, to all primaries, regardless of colour (top row) to red primaries (middle row) and to blue primaries (bottom row). The details of the separation between red and blue galaxies are given in Section 2.2.

Several strong trends are visible in these plots, both in the SDSS data and in the two models. More massive primary galaxies have systematically redder satellites (from left to right the curves and symbols go from dark blue to red in every panel of Figs 16 and 17). More massive satellites tend to be redder, at least for the two mass ranges considered here (curves and symbols shift rightward moving from the left-hand panel to the right-hand panel in each row). For all four primary mass ranges and for both satellite mass

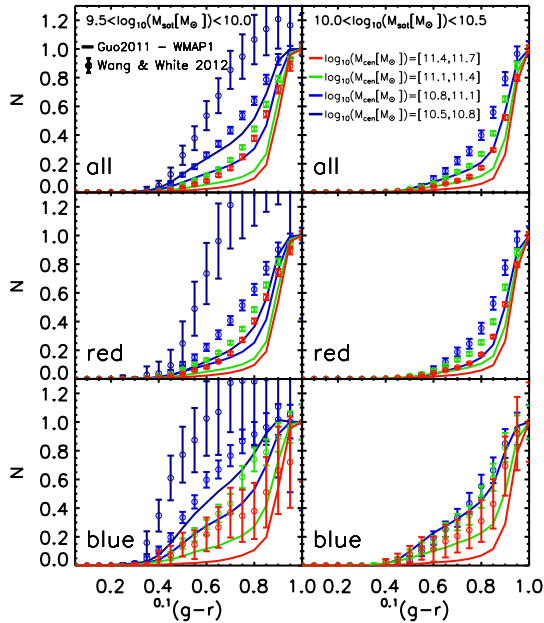


Figure 16. Cumulative $0.1(g-r)$ colour distributions for satellites projected within 300 kpc of their primaries. The Guo et al. (2011) model (solid lines) is compared with SDSS observations (symbols with error bars) for two different satellite stellar mass ranges (the left and right columns) around primaries in four different stellar mass ranges (indicated by the colours). In each case, results are given for the primary sample as a whole (in the top row) and for the sample split into red (middle row) and blue (lower row) primaries. The observational data in this plot are taken from fig. 12 of Wang & White (2012) while the model results are taken from their fig. 13.

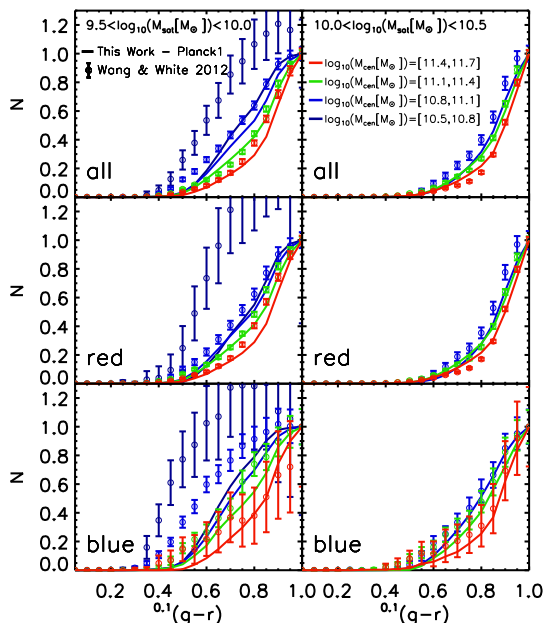


Figure 17. As Fig. 16 but now for our new model rather than that of Guo et al. (2011). Note that all the trends seen in the data and in the earlier model are also present in the new model, but that the satellite colour distributions are systematically shifted bluewards, bringing them into reasonable agreement with the SDSS data for all except low-mass satellites of the low-mass primaries.

ranges, red primaries have systematically redder satellites than blue primaries of the same stellar mass (the curves and symbols in every middle row panel lie to the right of the corresponding curves and symbols in the panel immediately below it). This last trend is the galactic conformity highlighted by Weinmann et al. (2006). For satellites projected within 300 kpc, it is clearly present both in the observations and in the models over a range of a factor of 20 in primary stellar mass and a factor of 10 in satellite stellar mass.

As pointed out by Wang & White (2012), in every panel of Fig. 16 the model curves lie well to the right of the corresponding symbols, showing that satellites are systematically too red in the Guo et al. (2011) model. As can be seen in Fig. 17, the situation is substantially improved in our new model where satellites are bluer in all cases and large discrepancies remain only for low-mass satellites of low-mass primaries. This is a result of the weaker impact of ram-pressure stripping, combined with the lowered threshold for star formation which allows satellites to keep forming stars for longer. It seems, nevertheless, that environmental effects are still too strong for low-mass satellites of low-mass primaries. As discussed in Wang et al. (2014), where an early version of the current model was found to produce radial distributions of blue satellites which are significantly less centrally concentrated than observed in the SDSS data, a possible solution may be to balance environmental effects with interaction-induced starbursts. These would enhance star formation in satellites close to orbital pericentre.

Wang & White (2012) argued that, in the model of Guo et al. (2011), conformity arises because red primaries have more massive haloes and more massive hot gas atmospheres than blue primaries of the same stellar mass, resulting in stronger environmental effects on their satellites. These effects are also present in our new model and may explain the strong quenching conformity between centrals and satellites found by Knobel et al. (2015) in their own analysis of SDSS data. On the other hand, Kauffmann et al. (2013) found conformity effects to persist out to projected distances of order 4 Mpc, considerably larger than the expected halo size of the central galaxies. They showed that although an effect of the same sign is present in the Guo et al. (2011) model, it is much weaker than observed. Hearin, Watson & van den Bosch (2015) and Hearin, Behroozi & van den Bosch (2016) show that small effects of the size seen in the model can be explained by the tendency of pairs of dark haloes at these separations to have correlated assembly histories. The origin of the strong effect seen by Kauffmann et al. (2013) remains uncertain, however. At these separations, conformity is actually somewhat weaker in our new model than in that of Guo et al. (2011). Kauffmann (2015) presents some evidence suggesting that a nongravitational process related to early AGN activity may be responsible for the observed effect.

7 SUMMARY

The current version of the Munich galaxy formation model, introduced in Henriques et al. (2015), applies the publicly available L-GALAXIES semi-analytic modelling code² to the Millennium and Millennium-II Simulations after scaling them to the *Planck* cosmology following Angulo & Hilbert (2015). The parameters of the galaxy formation model were adjusted to fit the observed variation of galaxy abundance and passive fraction as functions of stellar mass over the redshift range $0 \leq z \leq 3$. A good fit required significant modification of the physical assumptions underlying previous

² <http://galformod.mpa-garching.mpg.de/public/LGalaxies/>

public versions of the Munich models (Guo et al. 2011, 2013). In particular, to ensure that low-mass galaxies form most of their stars at $z < 1.5$ and are predominantly star-forming at $z = 0$, the ejection of material by SN feedback had to be increased and the reincorporation of ejected material had to be enhanced at late times (see Henriques et al. 2013). These changes increased star-formation rates at low redshift in low-mass central galaxies, but did not prevent such galaxies from turning red too quickly when they became satellites. The current model, in addition, reduces the cold gas density threshold for star formation and assumes ram-pressure stripping to be negligible in low-mass groups, thereby significantly increasing the fraction of low-redshift satellites with ongoing star formation. With these assumptions, intermediate mass galaxies continue to grow in mass at least down to $z \sim 1$. To ensure that they are nevertheless predominantly quenched by $z = 0$, it was necessary to change the scaling of AGN feedback to make it more efficient at late times.

In Paper I we showed that this new model agrees well at all redshifts with the observed stellar mass functions and passive fractions used to calibrate it. In Shamshiri et al. (2015), we developed new methods which retain detailed star formation histories for all galaxies at all redshifts. In combination with the population synthesis codes, these can be used (in post-processing) to obtain integrated spectra and magnitudes in arbitrary optical/near-infrared passbands for all objects. In Clay et al. (2015), we compared observed and modelled abundances and photometric properties at $4 \leq z \leq 7$, well beyond the redshift range used for calibration. In the current paper, we concentrate on the spatial distribution of galaxies in order to gauge how well our model represents the observed quenching of galaxies as a function of mass, environment and epoch. Quenching in the model is driven by AGN feedback, which suppresses gas accretion on to massive galaxies at the centres of hot gas haloes, and by environmental effects on satellite galaxies, namely the suppression of cosmological infall, the tidal stripping of haloes, and ram-pressure stripping in galaxy clusters. These processes interact in a complex way and it is important to replicate observational procedures closely in order to understand whether the observed trends are reproduced.

We began this paper by showing that when split by colour into star-forming and passive subsets the stellar mass functions of galaxies are a good fit to available observations over the full range $0 \leq z \leq 3$, and as a result they reproduce the phenomenology noted by Peng et al. (2010) over the more restricted range $0 \leq z \leq 1$ from their analysis of SDSS and COSMOS data. Namely that the SMF of star-forming galaxies evolves little with redshift and has a steep faint-end slope, while the SMF of passive galaxies has two components, one (corresponding to satellites) which has the same shape as that of star-forming galaxies and evolves equally slowly but at lower amplitude, and a second (corresponding to centrals) which has a much shallower low-mass slope and grows substantially in amplitude at low redshift. Even at fixed environment density (as estimated from the distance to the fifth nearest neighbour), passive fractions in the model vary with stellar mass at given redshift in a way which resembles that found by Peng et al. (2010). As a result, if we infer ‘mass quenching efficiencies’ from our model in the same way as they do from the data, we find results which are in qualitative agreement with theirs over the full range $0 < z < 1$, although the observationally inferred dependence on stellar mass is steeper than that in the model. This difference is also seen in a comparison with SDSS data as compiled by Wetzel et al. (2012), who split observed galaxies into ‘centrals’ and ‘satellites’ and used inferred halo mass as a measure of satellite environment. Another important outcome of our AGN-feedback-dependent quenching of massive galaxies is

that it naturally explains why these are observed to host more massive black holes when they are quenched than when they are still star-forming (Terrazas et al. 2016a).

Wetzel et al. (2012) explored the environment dependence of quenching in more detail by compiling SSFR histograms and radial profiles of passive fraction for satellite galaxies split according to stellar mass and halo mass. Our current model matches the SSFR histograms quite well for all stellar and halo masses, but is less successful in matching the radial profiles, which are significantly steeper than in the SDSS data. It appears that the radial dependence of quenching is overly strong in the model. On the other hand, the dependence of quenching on halo mass appears to be somewhat weaker in the model than in the Wetzel et al. (2012) compilation of SDSS data, although the qualitative agreement is quite good. For the Peng et al. (2010) definition of environment density, this problem shows up as a stronger dependence of quenched fraction on environment than is observed. The evolution of ‘environmental quenching efficiency’ in our model as defined by them is qualitatively similar to what they found, albeit with a stronger dependence on redshift.

The two-point statistics of galaxy clustering as a function of stellar mass/luminosity and colour/SSFR provide a well-established route to studying the environment dependence of galaxy formation and evolution. Observational determinations were already compared to predecessors of our current model in Springel et al. (2005) and Guo et al. (2011). The latter paper found agreement with low-redshift SDSS data to be good for massive galaxies and on large scales, but uncovered significant discrepancies at a small scale for low-mass galaxies, particularly for passive systems. This problem reflected an overly large passive fraction among satellite galaxies. The current model has decreased these discrepancies significantly, but to fully explore how clustering data depend on galaxy formation physics, it will be necessary to characterize better the observational uncertainties of the clustering measurements and to use them explicitly as constraints in the MCMC sampling of the galaxy formation parameter space (see van Daalen et al. 2016, for a first attempt in this direction). Two-point clustering data have recently become available at $z \sim 1$ and our current model agrees quite well with the autocorrelations as a function of stellar mass from DEEP2.

A particular aspect of galaxy two-point clustering statistics which has received considerable recent attention is the ‘conformity’ signal first pointed out by Weinmann et al. (2006). Satellites of passive central galaxies are more likely themselves to be passive than satellites of star-forming central galaxies of the same stellar mass. Kauffmann et al. (2013) pointed out that this signal extends out to companions at distances of several Mpc. These are too distant to be satellites as normally defined. We compared our model to the detailed information on satellite conformity compiled by Wang & White (2012) from SDSS data. As was the case for the Guo et al. (2011) model to which Wang & White (2012) compared, all the trends seen in the observations are qualitatively reproduced by the model. However, whereas the earlier model produced satellites that were systematically too red at all primary and satellite stellar masses, the distributions have shifted blue-ward in the new model and are in approximate agreement with the data for all but low-mass satellites of low-mass primaries.

As discussed by Wang & White (2012), strong satellite-central conformity arises in the model because passive centrals tend to have more massive haloes and more massive hot gas atmospheres than star-forming centrals of the same mass. The first effect is due to the fact that the haloes of star-forming centrals grow in parallel with the galaxy up to the present day whereas the haloes

of passive centrals continue to grow in mass after star formation has stopped. The second effect arises because the strength of AGN feedback increases with the mass of hot gas. These effects result in conformity because satellites are more likely to be quenched in more massive haloes with a denser gaseous atmosphere. Thus, halo mass and hot gas mass are acting as halo-wide ‘hidden variables’ of the kind which Knobel et al. (2015) inferred to be required in their own study of conformity. On the other hand, our new model is no better at reproducing the large-scale and strong apparent ‘two-halo conformity’ seen in the SDSS data than was the Guo et al. (2011) model used as comparison in the original Kauffmann et al. (2013) analysis.

Overall, the publicly available galaxy formation simulation presented in Paper I and further analysed here gives a good representation of the abundance and star formation distributions of galaxies over the full observed stellar mass range out to $z \sim 7$, as well as of galaxy clustering and the correlation of galaxy properties with environment out to $z \sim 1$. The clearest remaining discrepancies are the overly strong dependence of satellite quenching on halocentric radius, the lack of a strong two-halo conformity signal and the inability of our AGN feedback model to quench star formation in all galaxies with $\log_{10}(M_* [M_\odot]) \geq 11.0$ at low redshift (20 per cent of these have ongoing star formation). This last problem seems to be alleviated if we allow bar-driven accretion on to black holes. The advantages of our semi-analytic simulation and others like it over purely phenomenological models for the evolution of the galaxy population are that it automatically ensures consistency between the populations observed at different redshifts, and it allows observed trends to be interpreted directly in terms of physical processes. Its advantages over hydrodynamical simulations are that much larger volumes can be simulated, and that systematic exploration of the high-dimensional parameter space of galaxy formation is nevertheless feasible. Future work will undoubtedly bring further discrepancies to light and confirm the significance of those already identified. Exploring their origin should give additional insight into the astrophysics of galaxy formation and evolution.

ACKNOWLEDGEMENTS

This work used the DiRAC Data Centric system at Durham University, operated by the Institute for Computational Cosmology on behalf of the STFC DiRAC HPC Facility (www.dirac.ac.uk). This equipment was funded by BIS National E-infrastructure capital grant ST/K00042X/1, STFC capital grant ST/H008519/1, and STFC DiRAC Operations grant ST/K003267/1 and Durham University. DiRAC is part of the National E-Infrastructure. BMBH (ORCID 0000-0002-1392-489X) acknowledges support from a Zwicky Prize fellowship. The work of BMBH, SDMW and GL was supported by Advanced Grant 246797 ‘GALFORMOD’ from the European Research Council. PAT (ORCID 0000-0001-6888-6483) acknowledges support from the Science and Technology Facilities Council (grant number ST/L000652/1). REA acknowledges support from AYA2015-66211-C2-2. GQ acknowledges support from the NSFC grant (Nos. 11573033, 11622325), the Recruitment Program of Global Youth Experts of China, the NAOC grant (No. Y434011V01), MPG partner Group family and a Royal Society Newton Advanced Fellowship. The authors thank Ivan Baldry, Olivier Ilbert, Alexander Karim, Cheng Li, Danilo Marchesini and Adam Muzzin for providing their observational data; Eric Bell, Jarle Brinchmann, Guinevere Kauffmann, Bryan Terrazas, Stephen Wilkins and Rob Yates for useful discussions; and Claudia

Maraston, Gustavo Bruzual and Stephan Charlot for providing their stellar populations synthesis models.

REFERENCES

- Angulo R. E., Hilbert S., 2015, *MNRAS*, 448, 364
 Angulo R. E., White S. D. M., Springel V., Henriques B., 2014, *MNRAS*, 442, 2131
 Ann H. B., Park C., Choi Y.-Y., 2008, *MNRAS*, 389, 86
 Bahé Y. M., McCarthy I. G., 2015, *MNRAS*, 447, 969
 Baldry I. K., Balogh M. L., Bower R. G., Glazebrook K., Nichol R. C., Bamford S. P., Budavari T., 2006, *MNRAS*, 373, 469
 Benson A. J., Bower R. G., Frenk C. S., Lacey C. G., Baugh C. M., Cole S., 2003, *ApJ*, 599, 38
 Bernardi M., Meert A., Sheth R. K., Vikram V., Huertas-Company M., Mei S., Shankar F., 2013, *MNRAS*, 436, 697
 Blanton M. R., Roweis S., 2007, *AJ*, 133, 734
 Bluck A. F. L., Mendel J. T., Ellison S. L., Moreno J., Simard L., Patton D. R., Starkeburg E., 2014, *MNRAS*, 441, 599
 Bower R. G., Benson A. J., Malbon R., Helly J. C., Frenk C. S., Baugh C. M., Cole S., Lacey C. G., 2006, *MNRAS*, 370, 645
 Bower R. G., McCarthy I. G., Benson A. J., 2008, *MNRAS*, 390, 1399
 Bower R., Schaye J., Frenk C. S., Theuns T., Schaller M., Crain R. A., McAlpine S., 2016, *MNRAS*, 465, 32
 Bundy K., Ellis R. S., Conselice C. J., 2005, *ApJ*, 625, 621
 Caplar N., Lilly S. J., Trakhtenbrot B., 2015, *ApJ*, 811, 148
 Clay S. J., Thomas P. A., Wilkins S. M., Henriques B. M. B., 2015, *MNRAS*, 451, 2692
 Croton D. J. et al., 2006, *MNRAS*, 365, 11
 Daddi E. et al., 2007, *ApJ*, 670, 156
 Darvish B., Mobasher B., Sobral D., Rettura A., Scoville N., Faisst A., Capak P., 2016, *ApJ*, 825, 113
 Davis M., Geller M. J., 1976, *ApJ*, 208, 13
 Dressler A., 1980, *ApJ*, 236, 351
 Dubois Y., Volonteri M., Silk J., Devriendt J., Slyz A., Teyssier R., 2015, *MNRAS*, 452, 1502
 Elbaz D. et al., 2007, *A&AS*, 468, 33
 Faber S. M. et al., 2007, *ApJ*, 665, 265
 Font A. S. et al., 2008, *MNRAS*, 389, 1619
 Förster Schreiber N. M. et al., 2014, *ApJ*, 787, 38
 Gunn J. E., Tinsley B. M., 1976, *ApJ*, 210, 1
 Guo Q., White S., Li C., Boylan-Kolchin M., 2010, *MNRAS*, 404, 1111
 Guo Q. et al., 2011, *MNRAS*, 413, 101
 Guo Q., White S., Angulo R. E., Henriques B., Lemson G., Boylan-Kolchin M., Thomas P., Short C., 2013, *MNRAS*, p. 135
 Hartley W. G., Conselice C. J., Mortlock A., Foucaud S., Simpson C., 2015, *MNRAS*, 451, 1613
 Hearin A. P., Watson D. F., van den Bosch F. C., 2015, *MNRAS*, 452, 1958
 Hearin A. P., Behroozi P. S., van den Bosch F. C., 2016, *MNRAS*, 461, 2135
 Henriques B. M. B., Thomas P. A., 2010, *MNRAS*, 403, 768
 Henriques B. M., Bertone S., Thomas P. A., 2008, *MNRAS*, 383, 1649
 Henriques B. M. B., Thomas P. A., Oliver S., Roseboom I., 2009, *MNRAS*, 396, 535
 Henriques B., Maraston C., Monaco P., Fontanot F., Menci N., De Lucia G., Tonini C., 2011, *MNRAS*, 415, 3571
 Henriques B. M. B., White S. D. M., Lemson G., Thomas P. A., Guo Q., Marleau G.-D., Overzier R. A., 2012, *MNRAS*, 421, 2904
 Henriques B., White S., Thomas P., Angulo R., Guo Q., Lemson G., Springel V., 2013, *MNRAS*, 431, 3373
 Henriques B. M. B., White S. D. M., Thomas P. A., Angulo R., Guo Q., Lemson G., Springel V., Overzier R., 2015, *MNRAS*, 451, 2663
 Hopkins A. M., Beacom J. F., 2006, *ApJ*, 651, 142
 Hubble E. P., 1936, *Realm of the Nebulae*. Yale Univ. Press, New Haven
 Ilbert O. et al., 2010, *ApJ*, 709, 644
 Ilbert O. et al., 2013, *A&A*, 556, A55
 Karim A. et al., 2011, *ApJ*, 730, 61
 Kauffmann G., 2015, *MNRAS*, 454, 1840

- Kauffmann G. et al., 2003a, MNRAS, 341, 33
 Kauffmann G. et al., 2003b, MNRAS, 346, 1055
 Kauffmann G., White S. D. M., Heckman T. M., M nard B., Brinchmann J., Charlot S., Tremonti C., Brinkmann J., 2004, MNRAS, 353, 713
 Kauffmann G., Li C., Heckman T. M., 2010, MNRAS, 409, 491
 Kauffmann G., Li C., Zhang W., Weinmann S., 2013, MNRAS, 430, 1447
 Knobel C., Lilly S. J., Woo J., Kovac K., 2015, ApJ, 800, 24
 Kravtsov A., Vikhlinin A., Meshcheryakov A., 2014, ArXiv e-prints
 Larson R. B., Tinsley B. M., Caldwell C. N., 1980, ApJ, 237, 692
 Li C., Kauffmann G., Jing Y. P., White S. D. M., B rner G., Cheng F. Z., 2006, MNRAS, 368, 21
 Li C. et al., 2012, MNRAS, 419, 1557
 Lilly S. J., Le Fevre O., Hammer F., Crampton D., 1996, ApJ, 460, L1
 Luo Y., Kang X., 2016, RA&A, 17, 12
 Madau P., Ferguson H. C., Dickinson M. E., Giavalisco M., Steidel C. C., Fruchter A., 1996, MNRAS, 283, 1388
 Mandelbaum R., Wang W., Zu Y., White S., Henriques B., More S., 2016, MNRAS, 457, 3200
 Maraston C., 2005, MNRAS, 362, 799
 McGee S. L., Balogh M. L., Bower R. G., Font A. S., McCarthy I. G., 2009, MNRAS, 400, 937
 McGee S. L., Bower R. G., Balogh M. L., 2014, MNRAS, 442, L105
 Menci N., Fontana A., Giallongo E., Grazian A., Salimbeni S., 2006, ApJ, 647, 753
 Mo H. J., White S. D. M., 2002, MNRAS, 336, 112
 Moore B., Katz N., Lake G., Dressler A., Oemler A., 1996, Nat., 379, 613
 Mostek N., Coil A. L., Cooper M., Davis M., Newman J. A., Weiner B. J., 2013, ApJ, 767, 89
 Muzzin A. et al., 2013, ApJ, 777, 18
 Nantais J. B. et al., 2016, MNRAS, 594, 172
 Noeske K. G. et al., 2007, ApJ, 660, L43
 Oppenheimer B. D., Dav r R., 2008, MNRAS, 387, 577
 Oppenheimer B. D., Dav r R., Kere s D., Fardal M., Katz N., Kollmeier J. A., Weinberg D. H., 2010, MNRAS, 406, 2325
 Peebles P. J. E., 1988, Galaxy Formation: High Redshift or Low?. Kluwer, Dordrecht, the Netherlands
 Peng Y.-j. et al., 2010, ApJ, 721, 193
 Peng Y.-j., Lilly S. J., Renzini A., Carollo M., 2012, ApJ, 757, 4
 Phillips J. I., Wheeler C., Boylan-Kolchin M., Bullock J. S., Cooper M. C., Tollerud E. J., 2014, MNRAS, 437, 1930
 Planck Collaboration, 2014, A&AS, 571, A16
 Pozzetti L. et al., 2010, A&AS, 523, A13
 Prescott M. et al., 2011, MNRAS, 417, 1374
 Sales L. V. et al., 2015, MNRAS, 447, L6
 Schaye J. et al., 2010, MNRAS, 402, 1536
 Schaye J. et al., 2015, MNRAS, 446, 521
 Schechter P., 1976, ApJ, 203, 297
 Shamshiri S., Thomas P. A., Henriques B. M., Tojeiro R., Lemson G., Oliver S. J., Wilkins S., 2015, MNRAS, 451, 2681
 Somerville R. S., Hopkins P. F., Cox T. J., Robertson B. E., Hernquist L., 2008, MNRAS, 391, 481
 Springel V. et al., 2005, Nature, 435, 629
 Terrazas B. A., Bell E. F., Henriques B. M. B., White S. D. M., Cattaneo A., Woo J., 2016a, ApJ, 830, L12
 Terrazas B. A., Bell E. F., Henriques B. M. B., White S. D. M., 2016b, MNRAS, 459, 1929
 van Daalen M. P., Henriques B. M. B., Angulo R. E., White S. D. M., 2016, MNRAS, 458, 934
 Vogelsberger M. et al., 2014, Nature, 509, 177
 Wang W., White S. D. M., 2012, MNRAS, 424, 2574
 Wang J., De Lucia G., Kitzbichler M. G., White S. D. M., 2008, MNRAS, 384, 1301
 Wang L., Weinmann S. M., Neistein E., 2012, MNRAS, p. 2472
 Wang W., Sales L. V., Henriques B. M. B., White S. D. M., 2014, MNRAS, 442, 1363
 Weinmann S. M., van den Bosch F. C., Yang X., Mo H. J., 2006, MNRAS, 366, 2
 Weinmann S. M., van den Bosch F. C., Yang X., Mo H. J., Croton D. J., Moore B., 2006, MNRAS, 372, 1161
 Weinmann S. M., Kauffmann G., von der Linden A., De Lucia G., 2010, MNRAS, 406, 2249
 Weinmann S. M., Pasquali A., Oppenheimer B. D., Finlator K., Mendel J. T., Crain R. A., Macci o A. V., 2012, MNRAS, 426, 2797
 Wetzel A. R., Tinker J. L., Conroy C., 2012, MNRAS, 424, 232
 Wetzel A. R., Tinker J. L., Conroy C., van den Bosch F. C., 2013, MNRAS, 432, 336
 White S. D. M., 1989, in Frenk C. S., sEllis R. S., Shanks T., Heavens A. R., Peacock J. A., eds, NATO ASIC Proc. 264: The Epoch of Galaxy Formation Observable Signatures of Young Galaxies. p. 15
 White S. D. M., Frenk C. S., 1991, ApJ, 379, 52
 White S. D. M., Rees M. J., 1978, MNRAS, 183, 341
 Wilkins S. M., Trentham N., Hopkins A. M., 2008, MNRAS, 385, 687
 Woo J., Dekel A., Faber S. M., Koo D. C., 2015, MNRAS, 448, 237
 Yang X., Mo H. J., van den Bosch F. C., 2009, ApJ, 693, 830
 Zehavi I. et al., 2011, ApJ, 736, 59

APPENDIX A: COLOR CUTS

In this appendix we present the details of the different selections between active/blue and passive/red galaxies used throughout the paper. As explained in Section 2.2, these correspond to cuts in $u - r$ versus r , in $U - V$ versus $V - J$ (Fig. A1), in $U - B$ versus stellar mass (Fig. A2) and in $g - r$ versus stellar mass (Fig. A3). Table A1 summarizes where in the paper the different cuts were used.

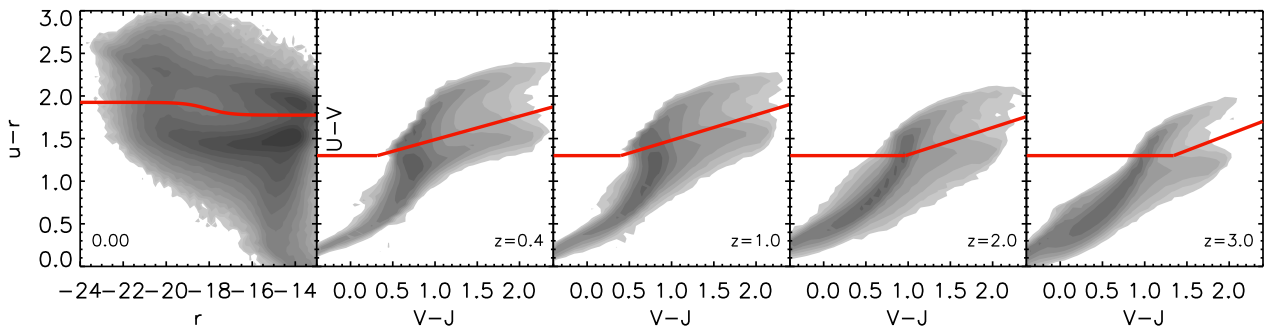
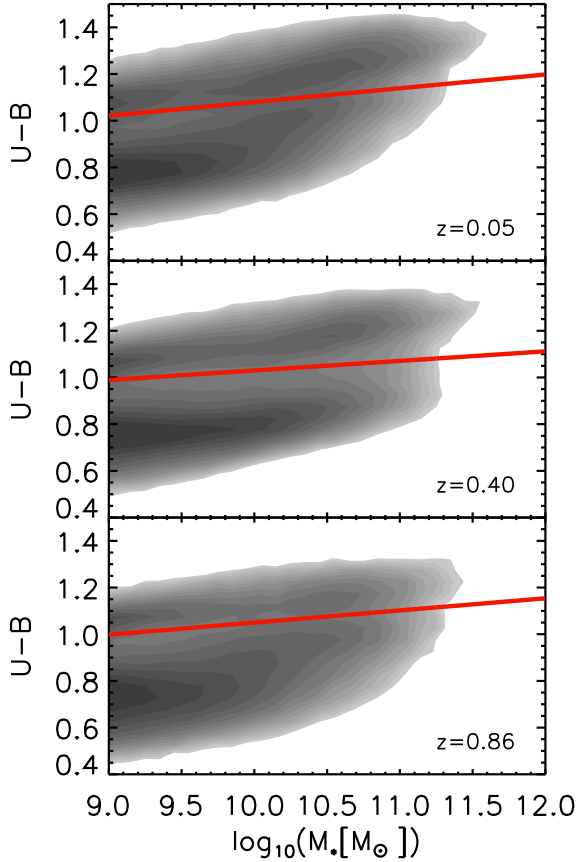
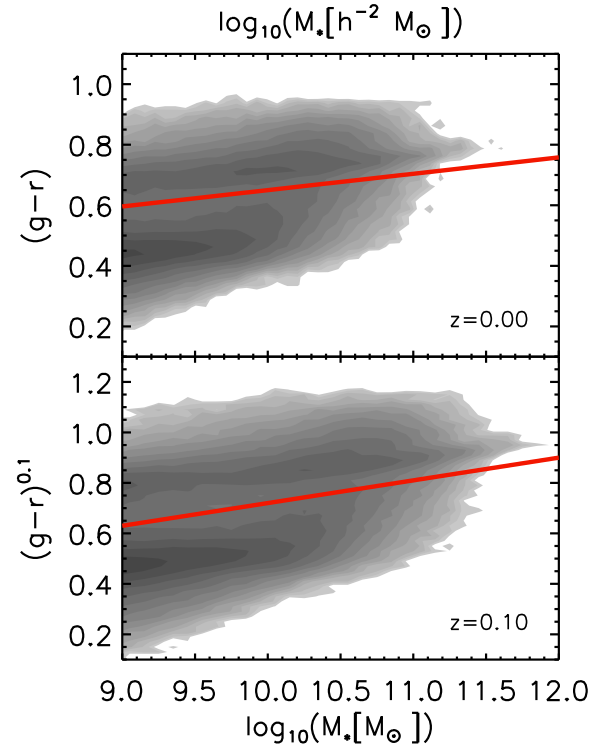


Figure A1. A cut at $u - r = 1.85 - 0.075 \times \tanh((M_r + 18.07)/1.09)$, at $z = 0$ (left-hand panel), and in the UVJ colour plane at higher redshifts (other panels). The division between populations corresponds to $U - V = 1.3$ and $(U - V) = (V - J) \times a(z) + b(z)$, where $a(z) = [0.28, 0.30, 0.32, 0.38]$ and $b(z) = [1.21, 1.18, 0.99, 0.79]$, respectively, at $z = 0.4, 1.0, 2.0$ and 3.0 .

Table A1. Summary of the cuts between active/blue and passive/red galaxies used in different figures in the paper.

| Cut between active/blue and passive/red galaxies | Used in |
|---|------------------------------|
| $u - r = 1.85 - 0.075 \times \tanh((M_r + 18.07)/1.09)$ | Figs 1 and 2 ($z = 0$) |
| $U - V = 1.3$ and $(U - V) = (V - J) \times 0.28 + 1.21$ | Figs 1 and 2 ($z = 0.4$) |
| $U - V = 1.3$ and $(U - V) = (V - J) \times 0.30 + 1.18$ | Figs 1 and 2 ($z = 1.0$) |
| $U - V = 1.3$ and $(U - V) = (V - J) \times 0.32 + 0.99$ | Figs 1 and 2 ($z = 2.0$) |
| $U - V = 1.3$ and $(U - V) = (V - J) \times 0.38 + 0.79$ | Figs 1 and 2 ($z = 3.0$) |
| $U - B > \log_{10}(M_* [M_\odot]) \times 0.059 + 0.49$ | Figs 4 and 11 ($z = 0.05$) |
| $U - B > \log_{10}(M_* [M_\odot]) \times 0.041 + 0.62$ | Figs 4 and 11 ($z = 0.40$) |
| $U - B > \log_{10}(M_* [M_\odot]) \times 0.052 + 0.53$ | Figs 4 and 11 ($z = 0.86$) |
| $g - r > \log_{10}(M_* [h^{-2} M_\odot]) \times 0.054 + 0.11$ | Figs 13, 14 and 15 |
| $(g - r)^{0.1} > \log_{10}(M_* [M_\odot]) \times 0.09 - 0.18$ | Figs 16 and 17 |


Figure A2. A selection in $U - B$ versus stellar mass. Red galaxies are defined to have $U - B > \log_{10}(M_* [M_\odot]) \times a(z) + b(z)$, where $a(z) = [0.059, 0.041, 0.052]$ and $b(z) = [0.49, 0.62, 0.53]$ (respectively at $z = 0.05, 0.40$ and 0.86).

Figure A3. A selection in $g - r$ versus stellar mass. Red galaxies are those with $g - r > \log_{10}(M_* [h^{-2} M_\odot]) \times 0.054 + 0.11$ (top panel) and $(g - r)^{0.1} > \log_{10}(M_* [M_\odot]) \times 0.09 - 0.18$ (bottom panel).

 This paper has been typeset from a \LaTeX file prepared by the author.